Experimental and Computational Study of the Transformation of Terminal Alkynes to Vinylidene Ligands on *trans*-(Chloro)bis(phosphine)Rh Fragments and Effects of Phosphine Substituents

Douglas B. Grotjahn,*[,†] Xi Zeng,[†] Andrew L. Cooksy,[†] W. Scott Kassel,[‡] Antonio G. DiPasquale,[‡] Lev. N. Zakharov,[‡] and Arnold L. Rheingold[‡]

Department of Chemistry and Biochemistry, 5500 Campanile Drive, San Diego State University, San Diego, California 92182-1030, and Department of Chemistry and Biochemistry, University of California, San Diego, La Jolla, California 92093-0385

Received April 11, 2007

Experimental and computational evidence points to unimolecular transformation of terminal alkynes on the title Rh(I) metal fragments. Lack of isotopic scrambling in double-crossover experiments is inconsistent with a previously proposed bimolecular pathway. Focusing on a unimolecular manifold, alkyne binding to the metal forms the Rh(I) alkyne π-complex **2**, which isomerizes to the Rh(III) hydrido(alkynyl) species **4**, ultimately leading to Rh(I) vinylidene product **5**. In making alkyne-free precursors, use of heterocyclic ligand (*i*-Pr)$_2$PIm′ (**1b**, Im′ = 1-methyl-4-*tert*-butylimidazol-2-yl) led to species **8** with a labile P,N chelate, whereas a geometrically similar *o*-tolyl ligand suffered metalation at the methyl group and was unsuitable for alkyne transformation studies. Kinetic studies comparing **1b** and (*i*-Pr)$_2$PPh (**1c**) allowed determination of rate constants for the alkyne binding event and conversion of **2** to **5** (the latter, k_{2-5}, being 9.6 times faster for **1b**). Based on a scan of the two-dimensional reaction surface, combined density functional/molecular mechanics calculations predict that η^2-(C,H) alkyne complex **3** is in a fast equilibrium with the lower energy hydrido(alkynyl) complex **4**, and neither species is expected to be present at observable concentrations. Eyring model estimates of the rate constants from these computational data predict the available experimental values in this work to within a factor of 2 and the ratio of the rate constants k_{2-5} for **1b** and **1c** to within 10%. The calculations also agree with the qualitative observation that reaction rates are faster for both ligands **1b** and **1c** than for (*i*-Pr)$_3$P and predict that reactions using triphenylphosphine will be faster than those with (*i*-Pr)$_3$P. NMR coupling constants, particularly $^1J_{CC}$ values, were used to evaluate bonding and back-bonding in isotopomers of **2a**−**c** and **5a**−**c** derived from H^{13}C^{13}CH.

Introduction

Many organic transformations of importance and utility in both industrial-scale[1,2] and fine-chemical synthesis involve activation of hydrocarbon C−H bonds, a topic of intense and continuing interest.[3−9]

Such reactions offer the ability to change the size of carbon frameworks or add new and higher-value functional groups at carbon. In addition, the use of transition metal compounds enables dramatic changes both in the stability of coordinated hydrocarbon ligands and in the specificity of reactions on the ligand undergoing transformation. For example, in the gas phase, vinylidene (:C═CH$_2$) is at least 40 kcal mol^{-1} less stable than its isomer acetylene (HC≡CH),[10,11] whereas this relationship can be reversed on coordination of both species to a metal.[12] Moreover, depending on metal and ligands, the changes in reactivity at carbons on going from a free terminal alkyne to a coordinated vinylidene allow a wide variety of functionalizations at C1 of the former alkyne that are impossible to achieve on the alkyne itself. Furthermore, vinylidene complexes are emerging as useful catalysts for alkene and alkyne metathesis chemistry. For all of these reasons, the increasing importance of vinylidenes in organic synthesis,[13] organometallic catalysis, and materials chemistry is highlighted

* Corresponding author. E-mail: grotjahn@chemistry.sdsu.edu.
† San Diego State University.
‡ University of California, San Diego. X-ray crystal structures.

(1) Satterfield, C. N. *Heterogeneous Catalysis in Industrial Practice*, 2nd ed.; McGraw-Hill: New York, 1991.
(2) Weissermel, K.; Arpe, H.-J. *Industrial Organic Chemistry*, 2nd Revised and Extended Edition; VCH: New York, 1993.
(3) Crabtree, R. H. *J. Chem. Soc., Dalton Trans.* **2001**, 2437−2450.
(4) Ritleng, V.; Sirlin, C.; Pfeffer, M. *Chem. Rev.* **2002**, *102*, 1731−1770.
(5) Klei, S. R.; Golden, J. T.; Burger, P.; Bergman, R. G. *J. Mol. Catal. A: Chem.* **2002**, *189*, 79−94.
(6) Labinger, J. A.; Bercaw, J. E. *Nature* **2002**, *417*, 507−514.
(7) *Activation and Functionalization of C-H Bonds*; Goldberg, K. I., Goldman, A. S., Eds.; American Chemical Society: Washington, D.C., 2004; Vol. 885.
(8) *Handbook of C-H Transformations*; Dyker, G., Ed.; Wiley-VCH: Weinheim, Germany, 2005.
(9) Lersch, M.; Tilset, M. *Chem. Rev.* **2005**, *105*, 2471−2526.
(10) Ervin, K. M.; Ho, J.; Lineberger, W. C. *J. Chem. Phys.* **1989**, *91*, 5974−5992.
(11) Chen, Y.; Jonas, D. M.; Kinsey, J. L.; Field, R. W. *J. Chem. Phys.* **1989**, *91*, 3976−3987.
(12) Wakatsuki, Y. *J. Organomet. Chem.* **2004**, *689*, 4092−4109.
(13) In particular, for recent uses of Rh vinylidenes in synthesis: (a) Trost, B. M.; Rhee, Y. H. *J. Am. Chem. Soc.* **2003**, *125*, 7482−7483. (b) Kim, H.; Lee, C. *J. Am. Chem. Soc.* **2005**, *127*, 10180−10181. (c) Kim, H.; Lee, C. *J. Am. Chem. Soc.* **2006**, *128*, 6336−6337. (d) Chen, Y.; Lee, C. *J. Am. Chem. Soc.* **2006**, *128*, 15598−15599. (e) Trost, B. M.; McClory, A. *Angew. Chem., Int. Ed.* **2007**, *46*, 2074−2077.

10.1021/om700355r CCC: $37.00
Publication on Web 06/01/2007

Scheme 1. Mechanistic Alternatives for Alkyne-to-Vinylidene Transformations

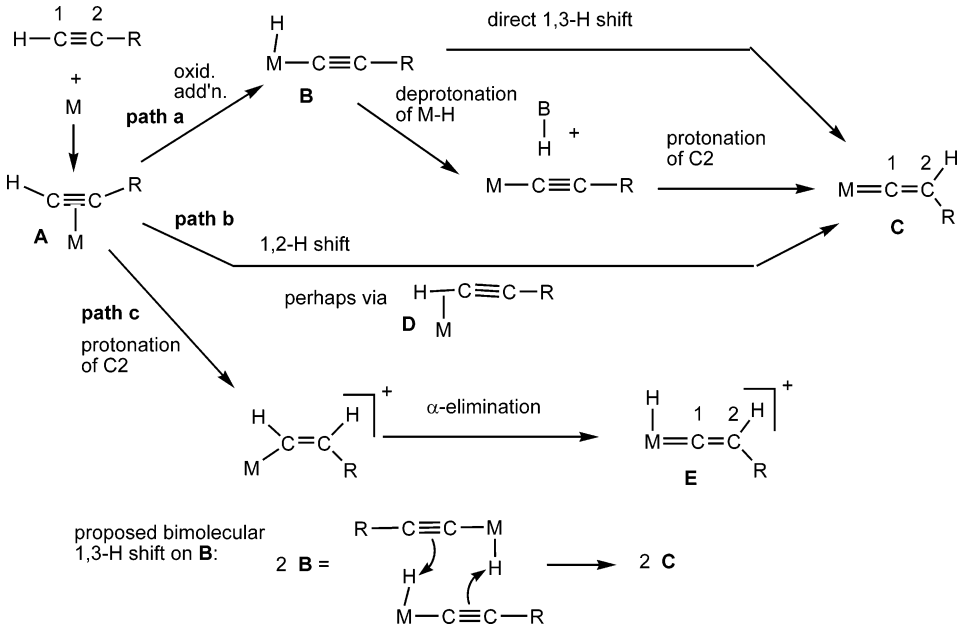

by the number and variety of recent reviews,[14−19] along with earlier ones.[20−24]

The utilization of novel alkyne and vinylidene reactivity in synthesis can be supported by studying the mechanism of alkyne-to-vinylidene transformation, a subject recently reviewed.[12] The first proposal of alkyne-to-vinylidene conversion on a metal was made in 1972.[25] Basic mechanistic alternatives shown in Scheme 1 all proceed from an initial alkyne−metal π complex (**A**). The first route (path a) involves oxidative addition of the alkyne C−H bond to give **B**, followed by a 1,3-shift of the hydride atom over the M−C1−C2 framework leading to **C**. One variant of this mechanism invokes deprotonation of the M−H unit and reprotonation at C2.[25,26] The second route (path b) features a direct 1,2-shift of the terminal C−H of the coordinated alkyne to C2, perhaps by way of an η^2-(C,H) complex (**D**).[27] Finally, a third possibility (path c) features initial protonation of coordinated alkyne in **A**, followed by 1,2-shift of the vinyl C−H toward the metal to give **E**.[28] One variant of this process starts with a preformed M−H species rather than requiring protonation.[29,30]

In our ongoing studies of catalytic alkyne transformations on CpRu fragments facilitated by an internal base within a phosphine ligand,[31−33] thus far we have found alkyne π-complexes to be elusive. This led us to study other metal fragments. A thorough series of pioneering synthetic papers from Werner and co-workers[34−39] showed that alkyne π-complexes of *trans*-(chloro)bis(phosphine)M (M = Rh, Ir) (e.g., **2**, Scheme 2) could be readily prepared using bulky, electron-rich phosphines such as (*i*-Pr)$_3$P (**1a**). More importantly, these species isomerized to vinylidene complexes **5** under moderate conditions (e.g., hours at 50 °C for Rh derivatives). Intriguingly, there were indications that added pyridine could either accelerate the conversion[37] or bind to the metal and allow trapping of hydrido(alkynyl) isomers of type **B**.[40] Finally, a major 1997 computational study[41] and some circumstantial evidence[37] suggested that the conversions of the latter compounds to vinylidenes followed an unusual bimolecular pathway (**B** to **C**, illustrated at the bottom of Scheme 1).

(14) Selegue, J. P. *Coord. Chem. Rev.* **2004**, *248*, 1543−1563.
(15) Katayama, H.; Ozawa, F. *Coord. Chem. Rev.* **2004**, *248*, 1703−1715.
(16) Valyaev, D. A.; Semeikin, O. V.; Ustynyuk, N. A. *Coord. Chem. Rev.* **2004**, *248*, 1679−1692.
(17) Werner, H. *Coord. Chem. Rev.* **2004**, *248*, 1693−1702.
(18) Bruneau, C.; Dixneuf, P. H. *Angew. Chem., Int. Ed.* **2006**, *45*, 2176−2203.
(19) Varela, J. A.; Saa, C. *Chem.−Eur. J.* **2006**, *12*, 6450−6456.
(20) Bruce, M. I.; Swincer, A. G. *Adv. Organomet. Chem.* **1983**, *22*, 59−128.
(21) Bruce, M. I. *Chem. Rev.* **1991**, *91*, 197−257.
(22) Dixneuf, P. H.; Bruneau, C.; Derien, S. *Pure Appl. Chem.* **1998**, *70*, 1065−1070.
(23) Bruneau, C.; Dixneuf, P. H. *Acc. Chem. Res.* **1999**, *32*, 311−323.
(24) Puerta, M. C.; Valerga, P. *Coord. Chem. Rev.* **1999**, *193−195*, 977−1025.
(25) Chisholm, M. H.; Clark, H. C. *J. Am. Chem. Soc.* **1972**, *94*, 1532−1539.
(26) Bianchini, C.; Peruzzini, M.; Vacca, A.; Zanobini, F. *Organometallics* **1991**, *10*, 3697−3707.
(27) Reviews on alkane complexes: Hall, C.; Perutz, R. N. *Chem. Rev.* **1996**, *96*, 3125−3146. Jones, W. D.; Vetter, A. J.; Wick, D. D.; Northcutt, T. O. In *Activation and Functionalization of C-H Bonds*; American Chemical Society: Washington DC, 2004; Vol. 885, pp 56−69. Recent leading references: Castro-Rodriguez, I.; Nakai, H.; Gantzel, P.; Zakharov, L. N.; Rheingold, A. L.; Meyer, K. *J. Am. Chem. Soc.* **2003**, *125*, 15734−15735. Lawes, D. J.; Geftakis, S.; Ball, G. E. *J. Am. Chem. Soc.* **2005**, *127*, 4134−4135. Lawes, D. J.; Darwish, T. A.; Clark, T.; Harper, J. B.; Ball, G. E. *Angew. Chem., Int. Ed.* **2006**, *45*, 4486−4490.
(28) Tokunaga, M.; Suzuki, T.; Koga, N.; Fukushima, T.; Horiuchi, A.; Wakatsuki, Y. *J. Am. Chem. Soc.* **2001**, *123*, 11917−11924.
(29) Olivan, M.; Eisenstein, O.; Caulton, K. G. *Organometallics* **1997**, *16*, 2227−2229.
(30) Olivan, M.; Clot, E.; Eisenstein, O.; Caulton, K. G. *Organometallics* **1998**, *17*, 3091−3100.
(31) Grotjahn, D. B.; Incarvito, C. D.; Rheingold, A. L. *Angew. Chem., Int. Ed.* **2001**, *40*, 3884−3887.
(32) Grotjahn, D. B.; Lev, D. A. *J. Am. Chem. Soc.* **2004**, *126*, 12232−12233.
(33) Grotjahn, D. B. *Chem.−Eur. J.* **2005**, *11*, 7146−7153.
(34) Alonso, F. J. G.; Höhn, A.; Wolf, J.; Otto, H.; Werner, H. *Angew. Chem., Int. Ed. Engl.* **1985**, *24*, 406−408.
(35) Werner, H.; Garcia Alonso, F. J.; Otto, H.; Wolf, J. *Z. Natursforsch., B* **1988**, *43b*, 722−726.
(36) Werner, H.; Brekau, U. *Z. Naturforsch., B* **1989**, *44b*, 1438−1446.
(37) Höhn, A.; Werner, H. *J. Organomet. Chem.* **1990**, *382*, 255−272.
(38) Werner, H.; Hampp, A.; Peters, K.; Peters, E. M.; Walz, L.; von Schnering, H. G. *Z. Naturforsch., B* **1990**, *45b*, 1548−1558.
(39) Canepa, G.; Brandt, C. D.; Werner, H. *Organometallics* **2001**, *20*, 604−606.
(40) Wolf, J.; Werner, H.; Serhadli, O.; Ziegler, M. *Angew. Chem., Int. Ed. Engl.* **1983**, *22*, 414−415.
(41) Wakatsuki, Y.; Koga, N.; Werner, H.; Morokuma, K. *J. Am. Chem. Soc.* **1997**, *119*, 360−366.

Scheme 2. Specific Ligands and Metal Complexes Considered in This Study

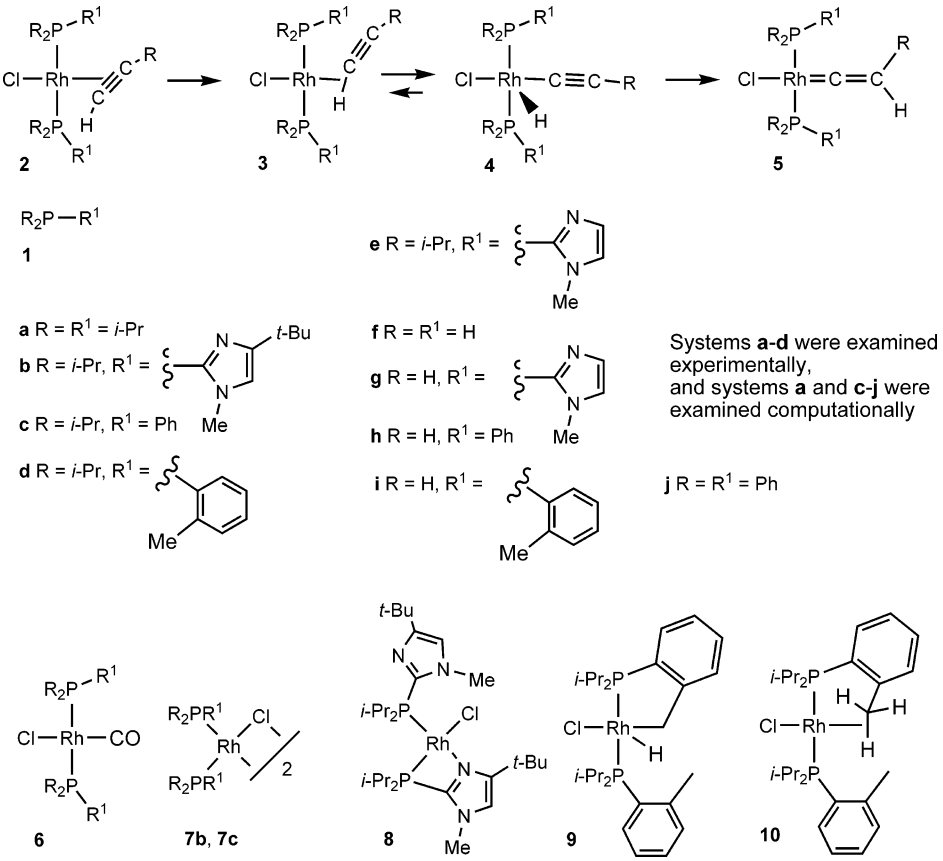

Therefore, we entered a study of Rh−alkyne and −vinylidene chemistry by preparing imidazolylphosphine **1b** as an analogue of **1a**. Remarkably, immediately on adding colorless **1b** and then 1-hexyne to a pale orange solution of Rh dimer [(μ-Cl)-Rh(cyclooctene)$_2$]$_2$, a deep permanganate-purple color appeared, and the resulting solution contained not the expected alkyne complex **2b** but rather its vinylidene isomer **5b**. This surprisingly rapid reaction (relative to that using **1a**) prompted the studies reported here. We recently made a preliminary report of experimental evidence from double-crossover experiments: the most significant finding was retention of isotopic composition, which was inconsistent with a bimolecular pathway from **B** to **C**.[42] Here we detail and expand on this experimental work and report a full computational study of the alkyne-to-vinylidene transformation.[43] In focusing on the unimolecular reaction pathway consistent with our experimental results, an η^2-(C,H) alkyne complex (**D**) emerged as a potential intermediate. In addition, we report a series of experiments and calculations elucidating the effects of the heterocycle, which in the case of chlorobis(phosphine)Rh(I) are minimal on the alkyne-to-vinylidene pathway but are profound on the structure and reactivity of alkyne-free precursors. Of more general significance, this paper also examines the steric and electronic effects of the phosphine substituents, a matter of increasing interest as synthetic applications continue to appear.[13]

Experimental Results and Discussion

Experimental Design. Our initial goal in this study was to elucidate the role of the phosphine heterocyclic substituent in the surprisingly rapid formation of a Rh vinylidene complex. Therefore, in addition to (i-Pr)$_2$PIm′ (**1b**, Im′ = 1-methyl-4-*tert*-butylimidazol-2-yl) we made two model ligands, (i-Pr)$_2$PPh (**1c**) and (i-Pr)$_2$P(o-Tol) (**1d**),[44] for comparison along with (i-Pr)$_3$P. The Ph ligand **1c** was chosen to be a closer electronic analogue to (i-Pr)$_2$PIm′ (**1b**) than **1a**, and the *o*-Tol analogue **1d** was chosen as an analogue electronically similar to **1c** with the additional steric contribution of the *ortho*-methyl group, designed to model the steric effect of the *N*-methyl group in **1b**.

With a total of four ligands (**1a**−**1d**) in hand, our major objectives were (1) to make *trans*-(chloro)(CO)[(i-Pr)$_2$PR]$_2$Rh complexes **6a**−**6d** and use the infrared stretching frequency of the CO ligand and solid-state bond lengths and angles as reporters of the steric and electronic effects of phosphine substituent R, (2) to make pure complexes of the form [(chloro)-((i-Pr)$_2$PR)$_2$Rh]$_n$ (n = 1 or 2) for alkyne binding studies, (3) to make authentic samples of alkyne and vinylidene complexes from these species, and (4) to study kinetics of alkyne transformation on Rh. Interesting effects of the heterocycle on precursor structure are described below. As our experimental study evolved, a fifth major objective became the synthesis and characterization of isotopically labeled alkyne and vinylidene complexes and crossover experiments involving the alkyne species. Not only did isotopic labeling prove decisive in determining the molecularity of alkyne-to-vinylidene transfor-

(42) Grotjahn, D. B.; Zeng, X.; Cooksy, A. L. *J. Am. Chem. Soc.* **2006**, *128*, 2798−2799.

(43) While this work was in progress, a computational study of alkyne-to-vinylidene transformation on the simple fragment *trans*-(chloro)Rh(PH$_3$)$_2$ appeared: Suresh, C. H.; Koga, N. *J. Theor. Comput. Chem.* **2005**, *4*, 59−73. No other phosphines were considered in this study.

(44) Riihimaki, H.; Kangas, T.; Suomalainen, P.; Reinius, H. K.; Jaaskelainen, S.; Haukka, M.; Krause, A. O. I.; Pakkanen, T. A.; Pursiainen, J. T. *J. Mol. Catal. A: Chem.* **2003**, *200*, 81−94.

Table 1. Comparison of Selected Data for *trans*-(chloro)(CO)[(*i*-Pr)$_2$PR^1]$_2$Rh (6)[a]

		infrared	NMR[b]		X-ray diffraction
complex	R^1	ν_{CO} (cm^{-1}, CH_2Cl_2)	$^{13}C\{^1H\}$ for CO ($CDCl_3$)	$^{31}P\{^1H\}$ ($CDCl_3$)	Rh−P (Å)
6a	*i*-Pr	1946[c]	189.0 (dt, J_{C-Rh} = 75.0, J_{C-P} = 15.0)	49.9 (J = 119.5)[d,48]	2.3488(3)[47]
6b	Im′	1966	186.4 (dt, J_{C-Rh} = 73.6, J_{C-P} = 15.5)	25.3 (J = 118.5)	2.3229(16)
6c	Ph	1965	187.3 (dt, J_{C-Rh} = 73.6, J_{C-P} = 15.3)	42.6 (J = 124.4)	2.3355(11)
6d	*o*-Tol	1960	186.8 (dt, J_{C-Rh} = 74.6, J_{C-P} = 15.4)	31.1 (J = 121.0)	2.3336(19)

[a] ^{31}P NMR and X-ray data for **6a** are from the literature cited, whereas all other values in Table 1 are from this work. [b] Chemical shifts in ppm, coupling constants in Hz. In $CDCl_3$ unless otherwise stated. [c] Literature values: 1950,[49] 1947,[47] 1946[50] (all in CH_2Cl_2), 1948 (CsI pellet),[51] 1943.2 (C_6D_6),[52] 1940 (matrix unspecified),[53] 1938 (Nujol).[48,54] [d] In C_6D_6.

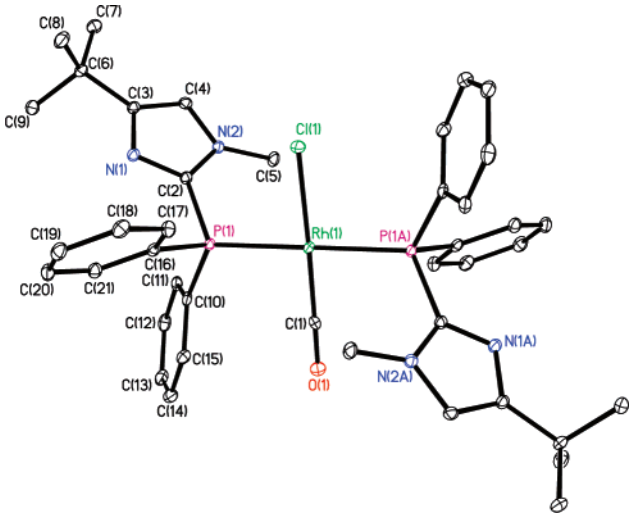

Figure 1. ORTEP view of **6b**, with ellipsoids shown at 30% probability. Only one position of the disordered Cl atom and CO ligand is shown for clarity.

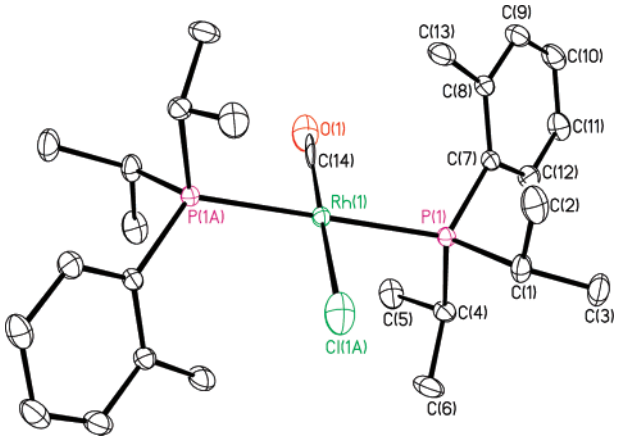

Figure 2. ORTEP view of **6d**, with ellipsoids shown at 30% probability. Only one position of the disordered Cl atom and CO ligand is shown for clarity.

mation, but it also allowed further characterization of metal−ligand back-bonding and hence effects of phosphine substituent R.

CO Complexes. Bubbling CO through a solution of the dimer [(μ-Cl)Rh(cyclooctene)$_2$]$_2$, followed by addition of (*i*-Pr$_2$)PR, evaporation of solvent, and recrystallization of the residue (which was essentially pure product containing some residual cyclooctene and solvent) afforded *trans*-(chloro)(CO)[(*i*-Pr)$_2$PR]$_2$Rh complexes **6b**−**6d** as yellow crystalline solids in 89−91% yields. The structures of the complexes and purities were verified by a combination of spectral data (key values of which are shown in Table 1), combustion analysis, and X-ray crystallography (Table 1 and Figures 1, 2, and S1).[45]

Inspection of IR data acquired in CH_2Cl_2 would suggest that the three ligands bearing one aromatic substituent have very similar properties,[46] close to being identical within experimental uncertainty. All three ligands are less electron-rich than the trialkylphosphine (*i*-Pr)$_3$P.[46]

In the crystal structures of **6b**−**6d**, because of the disorder of the Cl and CO ligands, a well-known phenomenon in structures of this general type,[47] determination of Rh−Cl, Rh−C, and C−O distances with precision needed to discuss subtle bonding changes is impossible. However, data not subject to this limitation are the Rh−P bond lengths for **6c** and **6d**, which are identical within experimental uncertainty (ca. 0.003 Å). For **6b**, this value is only 0.01 Å shorter than for **6c** and **6d**, whereas for **6a**, it is ca. 0.014 Å longer. These differences are only slightly greater than experimental uncertainties. In summary, the three aryl(di-isopropyl)phosphine ligands resemble each other as a group, distinct from (*i*-Pr)$_3$P.

Precursors for Study of Alkyne Binding and Transformation. From the work of Werner et al.,[55] the symmetrical dimer **7c** derived from (*i*-Pr)$_2$PPh is a known compound that is isolated as a violet solid in near-quantitative yield from the phosphine and [(μ-Cl)Rh(cyclooctene)$_2$]$_2$ in 4 to 1 molar ratio. In accord with literature data, its $^{31}P\{^1H\}$ NMR spectrum showed a sharp doublet at δ 58.9 ppm ($^1J_{RhP}$ = 197.7 Hz) in C_6D_6 and at 55.6 ppm in CD_2Cl_2.

In contrast, when (*i*-Pr)$_2$PIm′ and [(μ-Cl)Rh(cyclooctene)$_2$]$_2$ were combined in a molar ratio of 4 to 1 in CD_2Cl_2 or CH_2Cl_2, in addition to free cyclooctene, a single unsymmetrical species was seen, with two sharp $^{31}P\{^1H\}$ signals at 47.0 ppm (dd, $^1J_{RhP}$ = 181.1 Hz and $^2J_{PP}$ = 42.2 Hz) and 30.0 ppm (dd, $^1J_{RhP}$ = 162.6 Hz and $^2J_{PP}$ = 42.2 Hz). Structure **8** is consistent with the data. The upfield ^{31}P NMR signal with the smaller Rh−P coupling is assigned to the ^{31}P nucleus involved in the four-

(45) See Supporting Information for full details.

(46) For uses of Rh−CO stretching frequencies see: (a) Wang, K.; Goldman, M. E.; Emge, T. J.; Goldman, A. S. *J. Organomet. Chem.* **1996**, *518*, 55−68. (b) Huang, A.; Marcone, J. E.; Mason, K. L.; Marshall, W. J.; Moloy, K. G. *Organometallics* **1997**, *16*, 3377−3380. (c) Clarke, M. L.; Cole-Hamilton, D. J.; Slawin, A. M. Z.; Woollins, J. D. *Chem. Commun.* **2000**, 2065−2066. (d) Cooney, K. D.; Cundari, T. R.; Hoffman, N. W.; Pittard, K. A.; Temple, M. D.; Zhao, Y. *J. Am. Chem. Soc.* **2003**, *125*, 4318−4324. (e) Reference 47.

(47) Wilson, M. R.; Prock, A.; Giering, W. P.; Fernandez, A. L.; Haar, C. M.; Nolan, S. P.; Foxman, B. M. *Organometallics* **2002**, *21*, 2758−2763.

(48) Moigno, D.; Callejas-Gaspar, B.; Gil-Rubio, J.; Werner, H.; Kiefer, W. *J. Organomet. Chem.* **2002**, *661*, 181−190.

(49) Otto, S.; Roodt, A. *Inorg. Chim. Acta* **2004**, *357*, 1−10.

(50) Vastag, S.; Heil, B.; Marko, L. *J. Mol. Catal.* **1979**, *5*, 189−195.

(51) Intille, G. M. *Inorg. Chem.* **1972**, *11*, 695−702.

(52) Wang, K.; Rosini, G. P.; Nolan, S.; Goldman, A. S. *J. Am. Chem. Soc.* **1995**, *117*, 5082−5088.

(53) Busetto, C.; D'Alfonso, A.; Maspero, F.; Perego, G.; Zazzetta, A. *J. Chem. Soc., Dalton Trans.* **1977**, 1828−1834.

(54) Moigno, D.; Kiefer, W.; Callejas-Gaspar, B.; Gil-Rubio, J.; Werner, H. *New J. Chem.* **2001**, *25*, 1389−1397.

(55) Werner, H.; Kukla, F.; Steinert, P. *Eur. J. Inorg. Chem.* **2002**, 1377−1389.

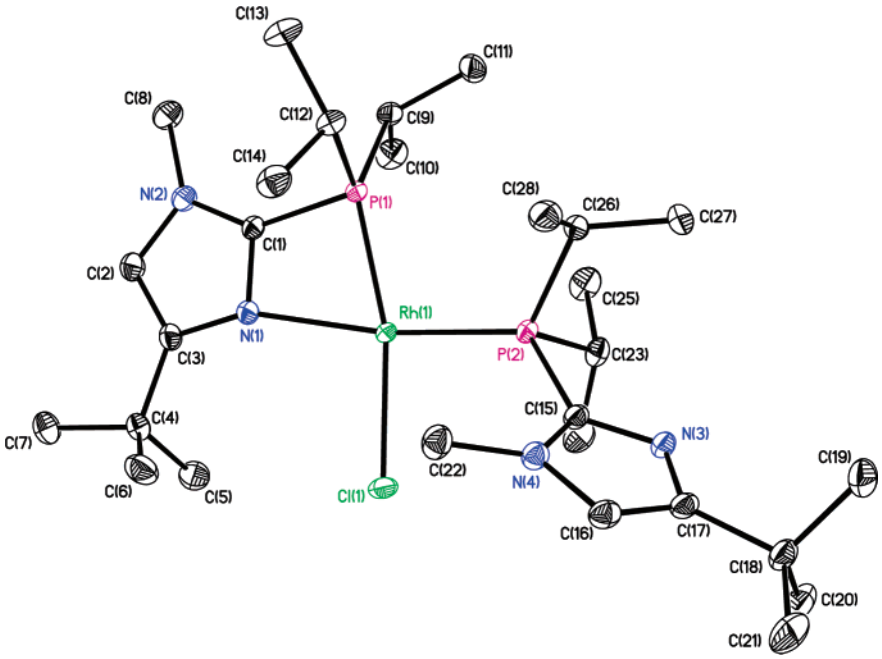

Figure 3. Molecular structure of **8**, with ellipsoids shown at 30% probability.

membered chelate.[56,57] Crystallization afforded pure **8** as a yellow solid in 95% yield.

The solid-state structure of **8** shown in Figure 3 confirms that there is a cis arrangement of phosphines in a distorted square-planar environment. The greatest deviation among the five atoms Rh, Cl, P, P, and N used to define a least-squares plane was seen by the Rh atom (0.0028 Å). Obvious distortions include the angle subtended by the chelate [P−Rh−N angle = 69.83(5)°] and the P−Rh−P angle of 101.694(18)°. Because almost identical distortions are seen even in a related (imidazole-2-thiolato)M complex,[58] in which the bulky $(i\text{-Pr})_2$P− group is replaced by a sterically undemanding S atom, these distortions are considered to be a consequence of the four-membered chelate rather than the size of the phosphine substituents.

The solid-state structure suggests hindrance to rotation about the Rh−P(2) bond caused by the pairs of *i*-Pr groups on each P as well as by the heterocyclic substituents. Indeed, cooling a CD_2Cl_2 solution of **8** in the NMR probe to −60 °C did not alter the already-sharp ^{31}P NMR resonances but did result in the appearance of four featureless ^{1}H NMR multiplets for the now-unique *i*-Pr methine protons, at δ 2.84, 2.48, 1.98, and 1.64 ppm. The signals near 1.2 ppm for the *i*-Pr methyls also changed in appearance but were overlapping and not well-resolved. Using line-shape analysis of ^{1}H NMR spectra observed between −80 and +30 °C, the barrier for rotation is calculated to be approximately 13 kcal mol^{-1}. A second dynamic process was indicated by observation of spectra at higher temperatures (between 30 and 105 °C, requiring THF-d_8 or toluene-d_8). Under these conditions, in ^{1}H and ^{31}P{^{1}H} NMR spectra of **8** changes indicative of coalescence of the two sets of resonances for the two imidazolylphosphines suggested the involvement of a fluxional exchange of the bound and free basic imidazole nitrogens, $\Delta H^{\ddagger}$ = 20.7 kcal mol^{-1} and $\Delta S^{\ddagger}$ = +13 eu. The positive $\Delta S^{\ddagger}$ value suggests a dissociative process.

All NMR spectra for **8** acquired in CD_2Cl_2 at temperatures ranging from 30 to −80 °C showed a single species whose NMR data were consistent with the solid-state structure shown in Figure 3, which is of relevance to the kinetics experiments described below, conducted at −20 °C in CD_2Cl_2. However, NMR data on solutions in less-polar solvents such as THF-d_8, benzene-d_6, and toluene-d_7 suggested equilibration of **8** with the minor, symmetrical species **7b** with spectral data and structure like that of dimer **7c**. Evaporation of the less-polar solvent containing **8** and **7b** and dissolution of the residue in CD_2Cl_2 led to complete conversion to **8**. Full details and discussion are in the Supporting Information.[45]

Whereas one of the heterocyclic nitrogens in **8** could occupy a coordination site on Rh(I), interaction of a ligand C−H bond was seen using $(i\text{-Pr})_2$P(*o*-Tol). When **1d** was combined with $[(\mu\text{-Cl})$Rh(cyclooctene$)_2]_2$ in a molar ratio of 4 to 1 in CD_2Cl_2, in addition to free cyclooctene, a major (ca. 80%) unsymmetrical species was seen, tentatively assigned structure **9**. As in the case of **8**, spectral data were consistent with the presence of two different phosphines; however, a large P−P coupling constant indicated trans orientation, as seen at 30 °C from two broadened ^{31}P{^{1}H} signals that sharpened at 0 °C to resonances at 72.3 ppm (dd, $^1J_{\mathrm{P-Rh}}$ = 119.2 Hz and $^2J_{\mathrm{P-P-trans}}$ = 367.5 Hz) and 39.1 ppm (dd, $^1J_{\mathrm{P-Rh}}$ = 111.5 Hz and $^2J_{\mathrm{P-P-trans}}$ = 367.5 Hz). The ^{1}H NMR spectrum at 0 °C showed a singlet at 1.95 ppm as expected for a methyl group on an aromatic ring, but the integral corresponded to *three* protons, not six. Moreover, at 0 °C there was a broad, featureless peak centered on −9.4 ppm integrating to approximately 2 H. Cooling the sample below 0 °C sharpened many of the ^{1}H NMR resonances, for example in the aromatic region, and importantly, upfield, revealing two broad, featureless one-proton peaks centered at −7.4 and −11.4 ppm. Spectra acquired on the same material dissolved in toluene-d_8 at various temperatures were more complex. Assignment as the oxidative addition product **9** was supported by the upfield ^{1}H NMR resonances and by observation in the infrared spectrum of a weak and slightly broad absorption centered at 2110 cm^{-1}, which was absent in an infrared spectrum of the ligand $(i\text{-Pr})_2$P-(*o*-Tol). This infrared stretch is more consistent with the presence

(56) Garrou, P. E. *Chem. Rev.* **1981**, *81*, 229−266.
(57) Grotjahn, D. B.; Gong, Y.; DiPasquale, A. G.; Zakharov, L. N.; Rheingold, A. L. *Organometallics* **2006**, *25*, 5693−5695.
(58) Miranda-Soto, V.; Perez-Torrente, J. J.; Oro, L. A.; Lahoz, F. J.; Martin, M. L.; Parra-Hake, M.; Grotjahn, D. B. *Organometallics* **2006**, *25*, 4374−4390.

of a Rh−H unit in **9** than of an agostic interaction in **10**.[59] Finally, in a simple study of reactivity, bubbling CO through a solution containing **9** did lead to a mixture containing **6d** as the major component, with spectral data identical to those presented above. However, overall, it was decided that because of uncertainty over the precise structure of the product from (*i*-Pr)$_2$P(*o*-Tol) and our inability to free it completely from impurities, or to get this mixture to react cleanly, the compound as obtained was unsuitable for kinetic studies described below. Nonetheless, it is interesting to contrast the activation of the methyl group on the aromatic ring of (*i*-Pr)$_2$P(*o*-Tol) with lack of such activation on (*i*-Pr)$_2$PIm′, in which the *N*-methyl group could in principle be metalated as was *N*-benzyl-2-diphenylphosphinoimidazole by Ir(I).[60] Interaction of a benzylic C−H bond ortho to an aromatic −PR$_2$ substituent through cyclometalation or agostic interaction is known for a variety of metals.[61−64] In contrast, the heterocyclic nitrogen in imidazolylphosphine **1b** offers an alternative way for a low-coordinate metal to achieve a ligand environment that is stable, but not too stable.

Alkyne Complexation and Vinylidene Formation. Synthetic Studies. At ambient temperatures, adding 1-hexyne to solutions of complexes **7c** and **8** led to formation of vinylidene complexes **5c-CCHBu** and **5b-CCHBu**, isolated as impressively deep violet solids. These species were also prepared in one pot, by first adding the appropriate phosphine to [(μ-Cl)Rh(cyclooctene)$_2$]$_2$, followed by 1-hexyne. Satisfactory combustion analyses were consistent with identity and purity of the samples. NMR spectral data diagnostic for the vinylidene ligand include downfield ^{13}C NMR resonances near δ 298 ppm with coupling to both Rh and P [for **5b-CCHBu**, δ 298.0 (td, $^2J_{C-P}$ = 17.4 Hz, $^1J_{C-Rh}$ = 55.2 Hz), for **5c-CCHBu**, 297.7 (td, $^2J_{C-P}$ = 17.4 Hz, $^1J_{C-Rh}$ = 55.2 Hz)] and upfield ^{1}H NMR resonances near 0 ppm for the Rh=C=C*H*CH$_2$CH$_2$CH$_2$CH$_3$ proton, which couples to Rh, the two P, and to neighboring methylene protons [for **5b-CCHBu**, δ 0.37 ppm (dtt, $^3J_{H-Rh}$ = 1 Hz, $^3J_{H-P}$ = 3.0 Hz, $^3J_{H-CH2}$ = 8 Hz, 1 H), for **5c-CCHBu** δ 0.00 ppm (dtt, $^3J_{H-Rh}$ = 1.8 Hz, $^3J_{H-P}$ = 3.5 Hz, $^3J_{H-CH2}$ = 8 Hz, 1 H)]. These data are in complete accord with those observed by Werner's group on many Rh(I) vinylidene complexes.[34−38,65]

Reaction of (*i*-Pr)$_2$PPh was slow enough at ambient temperatures to observe the intermediate π-alkyne complex **2c-HCCBu** by NMR, but to do so with the heterocyclic analogue required lowering the reaction temperature to −20 °C. In both cases the reactivity of 1-hexyne π-complexes **2b-** and **2c-HCCBu** precluded isolation, but for these species in the reaction mixture, diagnostic resonances for the terminal alkyne proton were found at 2.92 ppm for the (*i*-Pr)$_2$Ph case (**2c-HCCBu**) and 3.25 ppm for the (*i*-Pr)$_2$PIm′ case (**2b-HCCBu**) (dt = q, J = 2.5 Hz), along with in each case the appearance of a new doublet in the ^{31}P{^{1}H} NMR spectrum.

The identity of alkyne π-complexes and characterization of the bonding in these species were further secured by using doubly labeled acetylene, H−^{13}C^{13}C−H, to make **2b-** and **2c-H^{13}C^{13}CH**. In CD_2Cl_2 at −20 °C both H−^{13}C^{13}C−H complexes gave rise to ^{13}C NMR signals near 68 ppm showing coupling to both Rh and the two P [for (*i*-Pr)$_2$PPh complex δ 68.7 (dt, $^1J_{C-Rh}$ = 15.3 Hz, $^2J_{C-P}$ = 2.0 Hz) and for (*i*-Pr)$_2$PIm′ analogue δ 67.5 (dt, $^1J_{C-Rh}$ = 13.1 Hz, $^2J_{C-P}$ = 2.0 Hz)]. Notably, for the alkyne protons a 10-line pattern for the AA′XX′ system could be observed. Analysis of the pattern[45] in the case of the free alkyne as well as its complexes allowed determination of several coupling constants (Table 2), most significantly $^1J_{C-C}$, which was identical within experimental uncertainty (115.8−116.2 Hz) in the two complexes **2b-** and **2c-H^{13}C^{13}CH**.[66] The strong back-bonding of the metal to the alkyne π-system is obvious by noting that for the free alkyne, $^1J_{C-C}$ = 169.9 Hz, consistent with literature values of 165.8−173.6 Hz in various media.[67,68] There are extensive ^{13}C−^{13}C coupling data for organic molecules,[69−71] but fewer examples for metal complexes.[72] In this paper we are considering very closely related derivatives of the same alkyne, so it is reasonable to relate the magnitude of ^{13}C−^{13}C coupling to C−C distance[73,74] and hence the degree of metal−ligand back-bonding.[74] From data in Table 2 it is clear that the imidazol-2-yl and phenyl ligands are electronically very similar in this system. This conclusion was additionally supported (Table 2) by our data for a third system, (*i*-Pr)$_3$P complex **2a-H^{13}C^{13}CH**. In this complex, $^1J_{C-C}$ is definitely less (by ca. 1.5 Hz) than that seen in complexes

Table 2. Selected NMR Coupling Constants *J* (Hz) for H^{13}C^{13}CH and Complexes Derived from It, Relevant to Bonding in These Species[a]

	$^2J_{H-Rh}$	$^1J_{H-C}$	$^2J_{H-C}$	$^3J_{H-H}$	$^1J_{C-C}$	$^1J_{C-Rh}$
H^{13}C^{13}CH	na	248.8	49.6	9.6	169.9	na
2a-H^{13}C^{13}CH	2.5	229.7	28.0	1.7	114.6	16.0
2a-H^{13}C^{13}CH[b]	2.5	228.5	27.5	1.7	114.5	15.7
2b-H^{13}C^{13}CH	2.6[c]	232.9[c]	29.3[c]	1.7[c]	115.8[c]	14.7
2c-H^{13}C^{13}CH	2.5	232.8	29.0	1.8	116.2	nd
2c-H^{13}C^{13}CH[d]	2.5	233.2	29.1	1.7	115.8	15.3
5a-^{13}C^{13}CH$_2$[b]	na	161.7	na	na	57.0	57.0
5b-^{13}C^{13}CH$_2$	na	163.0	na	na	58.0	55.4
5c-^{13}C^{13}CH$_2$	na	163.0	na	na	58.7	55.6

[a] Data acquired on samples in CD_2Cl_2 at 30 °C unless otherwise indicated. "na" means not applicable. "nd" means not determined. [b] In C_6D_6. [c] At 20 °C. [d] At −20 °C.

(59) Brookhart, M.; Green, M. L. H. *J. Organomet. Chem.* **1983**, *250*, 395−408.
(60) Tejel, C.; Ciriano, M. A.; Jimenez, S.; Oro, L. A.; Graiff, C.; Tiripicchio, A. *Organometallics* **2005**, *24*, 1105−1111.
(61) Rheingold, A. L.; Fultz, W. C. *Organometallics* **1984**, *3*, 1414−1417.
(62) Herrmann, W. A.; Brossmer, C.; Reisinger, C.-P.; Riermeier, T. H.; Öfele, K.; Beller, M. *Chem.−Eur. J.* **1997**, *3*, 1357−1364.
(63) Baratta, W.; Del Zotto, A.; Herdtweck, E.; Vuano, S.; Rigo, P. *J. Organomet. Chem.* **2001**, *617−618*, 511−519.
(64) Sjoevall, S.; Andersson, C.; Wendt, O. F. *Organometallics* **2001**, *20*, 4919−4926.
(65) Werner, H.; Wolf, J.; Höhn, A. *J. Organomet. Chem.* **1985**, *287*, 395−407.
(66) The values given in this paper differ slightly from those appearing in our original communication,[42] because an empirical fitting of the data has now been supplanted by a rigorous analysis. See Experimental Section and Supporting Information for full details.
(67) Wigglesworth, R. D.; Raynes, W. T.; Kirpekar, S.; Oddershede, J.; Sauer, S. P. A. *J. Chem. Phys.* **2000**, *112*, 3735−3746.
(68) Jackowski, K.; Wilczek, M.; Pecul, M.; Sadlej, J. *J. Phys. Chem. A* **2000**, *104*, 5955−5958.
(69) Krivdin, L. B.; Kalabin, G. A. *Prog. Nucl. Magn. Reson. Spectrosc.* **1989**, *21*, 293−448.
(70) Kamienska-Trela, K. *Annu. Rep. NMR Spectrosc.* **1995**, *30*, 131−230.
(71) For experimental and computational studies of $^1J_{C-C}$ in acetylene derivatives, see refs 71a−f. (a) Sebald, A.; Wrackmeyer, B. *Spectrochim. Acta, Part A* **1981**, *37A*, 365−368. (b) Wrackmeyer, B. *Spectroscopy (Amsterdam, Netherlands)* **1982**, *1*, 201−208. (c) Lambert, J.; Klessinger, M. *Magn. Reson. Chem.* **1987**, *25*, 456−461. (d) Zinchenko, S. V.; Kalabin, G. A.; Krivdin, L. B.; Proidakov, A. G.; Bazhenov, B. N. *Zh. Org. Khim.* **1988**, *24*, 1595−1605. (e) Biedrzycka, Z.; Kamienska-trela, K. *Pol. J. Chem.* **2003**, *77*, 1637−1648. (f) Pecul, M.; Ruud, K. *Magn. Reson. Chem.* **2004**, *42 (Special Issue)*, S128−137.
(72) For studies of $^1J_{C-C}$ on metal complexes in general, see ref 69, pp 186−196. For dramatic differences between mono- and dinuclear alkyne−metal complexes, see in particular: Aime, S.; Osella, D.; Giamello, E.; Granozzi, G. *J. Organomet. Chem.* **1984**, *262*, C1−C4.
(73) Benn, R.; Rufinska, A. *Organometallics* **1985**, *4*, 209−214.
(74) Grotjahn, D. B.; Collins, L. S. B.; Wolpert, M.; Lo, H. C.; Bikzhanova, G. A.; Combs, D.; Hubbard, J. L. *J. Am. Chem. Soc.* **2001**, *123*, 8260−8270.

Scheme 3. Results of Crossover Experiments Forming 5[a]

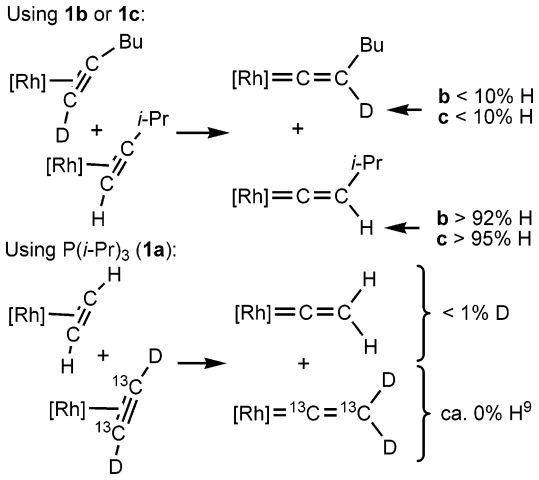

[a] Upper bounds given are estimated detection limits.

derived from the other two ligands, following the trends in the infrared stretching frequency in the corresponding CO complexes (Table 1). In fact, although the focus of attention here has been on $^1J_{C-C}$, by looking at the data in Table 2, one can see from the other coupling constants of sufficient magnitude ($^1J_{H-C}$, $^2J_{H-C}$, and even $^1J_{C-Rh}$) that the values for the imidazol-2-yl and phenyl derivatives are identical within experimental uncertainty or nearly so, and distinct from those for **2a-H^{13}C^{13}CH**.

The doubly labeled acetylene complexes evolved to the corresponding vinylidenes **5a-**, **5b-**, and **5c-^{13}C^{13}CH$_2$**, which were characterized in solution by several key NMR resonances. The ^{13}C NMR spectrum of the Ph analogue **5c-^{13}C^{13}CH$_2$** showed two strong mutually coupled ($^1J_{C-C}$ = 58.7 Hz) peaks at δ 297.9 ($^2J_{C-P}$ = 17.1 Hz, $^1J_{C-Rh}$ = 55.6 Hz) and 90.7 ppm ($^3J_{C-P}$ = 6.5 Hz, $^2J_{C-Rh}$ = 15.7 Hz) for C1 and C2 of the Rh=^{13}C=^{13}CH$_2$ unit. Similar data were found for the Im′ analogue. Most significantly, the value of $^1J_{C-C}$ in both systems (58.7 and 58.0 Hz) was virtually identical, again suggesting virtually identical C−C bond distances and hence metal−vinylidene back-bonding (Table 2),[75] especially considering that the same parameter had a value of 57.0 Hz for the (*i*-Pr)$_3$P analogue.

In our work, all attempts to detect hydrido(alkynyl) isomers **4** or other intermediates in conversions of alkyne complexes to vinylidenes were unsuccessful. The conversions of **2b-** and **2c-H^{13}C^{13}CH** to the corresponding vinylidene isomers were not completely clean, particularly if less than 1 equiv of labeled alkyne was used and some unreacted **8** or **7c** was present. More conclusive results regarding the absence of detectable amounts of **4** came from careful examination of reactions of **8** and **7c** with 1-hexyne, which showed only alkyne-free precursor **8** or **7c**, corresponding alkyne π-complex **2b-HCCBu** or **2c-HCCBu**, and final vinylidene **5b-CCHBu** or **5c-CCHBu**. It could be estimated that the lower detection limit in these latter experiments was from 1% to 5%. Computational and kinetics results (*vide infra*) are consistent with our inability to detect hydride complexes **4** or other reaction intermediates at these levels.

Crossover Experiments. In order to determine the molecularity of the conversion of hydrido(alkynyl) intermediate **4** to vinylidene product **5**, we turned to a series of double-crossover experiments on isotopically labeled species (Scheme 3).

We note that a double-crossover experiment was attempted on hydrido(alkynyl)iridium species like **4a**, but unfortunately, rapid H−D exchange between the hydridic starting materials prevented a conclusion regarding molecularity.[37] In our work, adding an equimolar mixture of terminal alkynes DCC(CH$_2$)$_3$CH$_3$ and HCCCHMe$_2$ (0.6 equiv of each relative to the amount of Rh) to either **7c** or **8** at −20 °C produced mixtures of alkyne π-complexes **2**, which evolved to vinylidene complexes (**5**) as the mixtures were warmed. *Significantly, with an estimated detection limit of 5−10%, no crossover was detected, regardless of ligand type,* inconsistent with significant bimolecular 1,3-H shift. We note that Li and Crabtree performed similar crossover experiments on a (hydrido)Ir(III) system and observed a lack of crossover in products derived from alkyne-to-vinylidene transformation at some stage.[76,77]

However, because the propensity for bimolecular reaction could be a function of hindrance on the alkyne or the phosphine, and because the previous studies[37,41] focused on acetylene itself and the (*i*-Pr)$_3$P ligand, we allowed a 1:1 mixture of **2a-HCCH** and **2a-D^{13}C^{13}CD** to convert to vinylidene complexes **3** at 25−30 °C in C_6D_6. Remarkably, formation of **5a-CCH$_2$** and **5a-^{13}C^{13}CD$_2$** is consistent with an absence of crossover even in this system. Notably, our estimated limit of detection of D in **5a-CCH$_2$** is 1%. *The absence of isotopomer **5a-CCHD** from **2a-HCCH** in the presence of the D^{13}C^{13}CD isotopomer is the most compelling evidence against crossover.*

Surprisingly, the rearrangement of pure **2a-D^{13}C^{13}CD** in silylated and dried NMR tubes gave **5a-^{13}C^{13}CD$_2$** along with 10−20% of the ^{13}C^{13}CHD isotopomer **5a-^{13}C^{13}CHD**, which somewhat complicated the crossover analysis. In these experiments, the source of the H could not be determined, but it would not appear to be extraneous water, because the amount of H incorporation was unaffected by pretreating the NMR tube with D_2O before drying or by the presence or absence of **2a-HCCH**. Moreover, the vinylidene protons of **5-CCH$_2$** did not exchange with D_2O at room temperature in C_6D_6. Finally, we ruled out the role of a kinetic isotope effect by observing that separate solutions of **2a-D^{13}C^{13}CD** and **2a-HCCH** rearrange to the respective vinylidenes at 30 °C in the NMR probe. Comparing rates of disappearance of starting materials showed that $k_{HCCH}/k_{D13C13CD}$ = 1.67, a relatively small effect compared with the low or undetectable D incorporation in crossover experiments above. Katayama and co-workers found k_{PhCCH}/k_{PhCCD} = 1.69(5) for similar transformation on a Ru(II) center.[15]

Kinetics. A series of kinetics experiments was undertaken with the goals of determining microscopic rate constants and evaluating the effects of the heterocyclic ligand on each step of alkyne-to-vinylidene transformation. To a cooled solution of precursor **8** or **7c** in CD_2Cl_2 was added 1-hexyne, and the resulting cold NMR tube was inserted into an NMR probe precooled to −20 °C. The evolution of the mixture from alkyne-free precursor and 1-hexyne to alkyne complex **2-HCCBu** to vinylidene complex **5-CCHBu** was followed by ^{1}H NMR. The rate constants for three elementary steps were then fit to the observed concentration versus time profiles: step 1 = alkyne binding to precursor, forming **2**; step 2 = transformation of **2** to the hydrido(alkynyl) species **4**; step 3 = transformation of **4** to **5**. For a given mechanism and set of rate constants, the concentrations were predicted as a function of time using a fourth-order Runge−Kutta numerical integration, and the rate

(75) The identity of the trans-ligand in (halo)(^{13}C^{13}CH$_2$)Rh[(*i*-Pr)$_3$P]$_2$ affects $^1J_{C-C}$; see ref 48. Apparently, in ref 48 the reported values of $^1J_{C-C}$ are off by a factor of 2.

(76) Li, X.; Incarvito, C. D.; Crabtree, R. H. *J. Am. Chem. Soc.* **2003**, *125*, 3698−3699.
(77) Li, X.; Vogel, T.; Incarvito, C. D.; Crabtree, R. H. *Organometallics* **2005**, *24*, 62−76.

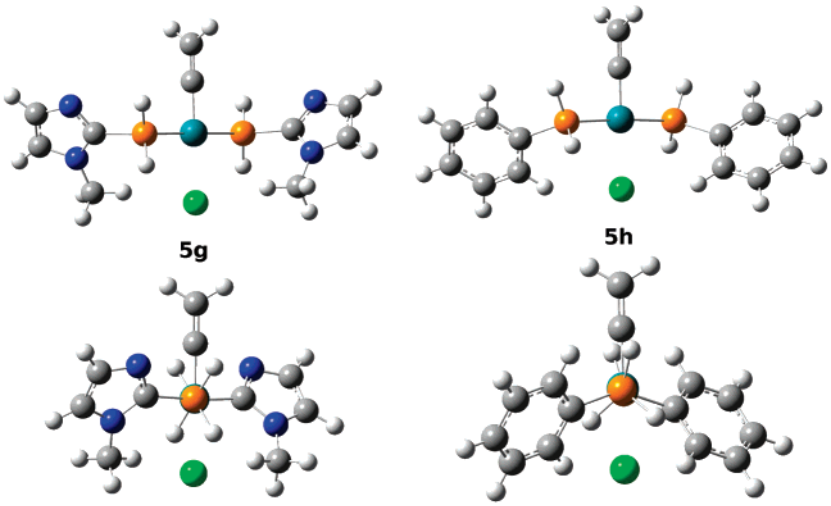

Figure 4. B3LYP/LANLDZ lowest energy conformers of **5g** and **5h**. In each case the upper view is from a point perpendicular to the P−P axis, whereas the lower one is from a point on the P−P axis, showing the *anti* orientation of aromatic groups.

constants were then iteratively optimized in a least-squares fit to the data. (These data do not differentiate between the unimolecular and bimolecular mechanisms for step 3, because if the unobserved intermediate **4** is in steady state, then the product formation rate is approximately proportional to the concentration of **2** for either mechanism.) The numerical integration predicts that the concentration of **4** never exceeds 0.002 mM in any of these experiments, consistent with its failure to be detected by NMR. As a result of this, however, the rate constants for steps 2 and 3 cannot be independently determined from the available data, and these were therefore combined into a single effective rate constant, k_{2-5}. For **8**, the rate constant for formation of **2** is $k = 9.52(23) \times 10^{-5}$ mM^{-1} min^{-1} and the *effective* rate constant for formation of **5** from **2** is $k_{2-5} = 3.32(22) \times 10^{-2}$ min^{-1}. For **7c**, $k = 2.01(65) \times 10^{-3}$ mM^{-1} min^{-1} and $k_{2-5} = 3.46(19) \times 10^{-3}$ min^{-1}. Thus, the rate constant k_{2-5} for the overall H-shift is 9.6 times greater with the heterocyclic system than with the nonheterocyclic one.

Conclusions from Experiments and Rationale for Calculations. Profound changes in complex structure as a function of ligand in this study are seen before addition of alkyne: the hybrid P,N-ligand **1b** leads to the fluxional chelate complex **8** with intact *N*-methyl substituents, whereas in **1d** lack of a potentially coordinating nitrogen leads to methyl metalation (**9**). In contrast, all available X-ray diffraction and IR and NMR spectral data on *trans*-chlorobis(phosphine)Rh(I)−L species (L = CO, H^{13}C^{13}CH, or vinylidene ^{13}C^{13}CH$_2$) highlight the *similarity* of ligands with either imidazol-2-yl (**1b**) or phenyl-derived (**1c**, **1d**) substituents, distinct from the (*i*-Pr)$_3$P case **1a**.

As for alkyne-to-vinylidene transformation, the crossover experiments on the isomerization of alkyne π-complexes on *trans*-(chloro)bis(phosphine)Rh are inconsistent with a bimolecular pathway leading to vinylidene complexes. Hydride intermediates were not detectable. For a given alkyne, the rearrangement appears to be fastest for (*i*-Pr)$_2$PR^1 where R^1 = aryl. The imidazolyl unit leads to a somewhat faster reaction, perhaps because of the hemilability[78−82] of the chelate in **8**, a process for which we have determined activation parameters. From the kinetics experiments, a 9.6-fold increase in alkyne-to-vinylidene conversion rate k_{2-5} was seen. Finally, the inability to detect hydride intermediates and follow their concentrations with time precluded determination of the rate law for the vinylidene-forming step or the microscopic rate constants for individual steps, so effects of the phosphine substituents had to be evaluated further using computational means.

Kang et al. computed the relative energies of the PH$_3$ species **2f**, **4f**, and **5f**, optimizing geometries at the MP2 level and calculating energies at the MP4 level.[83] Although they calculated the barrier for alkyne rotation in **2f**, they did not probe the kinetics of the reaction from **2** to **5**. The following year, Wakatsuki et al. 's detailed computational investigation of the reaction of **2f** and **2a**[41] employed a combination of the MP2 *ab initio* and MM3 molecular mechanics techniques, making the treatment of the *i*-Pr groups in **2a**, **4a**, and **5a** tractable. That work found barriers of over 30 kcal/mol to both steps (Scheme 1, **A** → **B** and **B** → **C**) of the unimolecular reaction, inconsistent with the observed rate of reaction and inspiring the proposal of a bimolecular 1,3-H shift mechanism shown at the bottom of Scheme 1. With the advantage of experiments inconsistent with a bimolecular mechanism, we therefore carried out a new computational investigation in an effort to describe the reaction mechanism in greater detail and shed light on the discrepancy between the experiments and previous calculations.

Computational Results and Discussion

The computational study consisted of (1) conformational analysis at the B3LYP/LANL2DZ level of the R^1 group orientations, (2) mapping of the B3LYP/LANL2DZ reaction surface that connects structures **2f**−**5f** in order to identify the relevant intermediates and transition states, (3) B3LYP/LANL2DZ geometry optimizations and frequency calculations for structures **2g**−**5i**, based on the previous conformational and reaction surface analyses, (4) geometry optimizations of structures **2a**−**5a**, **2c**−**5c**, **2d**−**5d**, and **2e**−**5e** by BLYP/DQZ/UFF ONIOM calculations (henceforth "BDMM"). Details surrounding these steps and the choice of methods are given in the Experimental Section. The most stable conformations identified in all cases are characteristic of a stabilizing interaction between the R^1 group and Cl atom, as exemplified in Figure 4. Calculations on conformers of **5g** as well as on prior intermedi-

(78) Braunstein, P. *J. Organomet. Chem.* **2004**, *689*, 3953−3967.
(79) Werner, H. *Dalton Trans.* **2003**, 3829−3837.
(80) Braunstein, P.; Naud, F. *Angew. Chem., Int. Ed.* **2001**, *40*, 680−699.
(81) Börner, A. *Eur. J. Inorg. Chem.* **2001**, 327−337.
(82) Schneider, J. J. *Nachr. Chem.* **2000**, *48*, 614−616, 618−620.
(83) Kang, S. K.; Song, J. S.; Moon, J. H.; Yun, S. S. *Bull. Kor. Chem. Soc.* **1996**, *17*, 1149−1153.

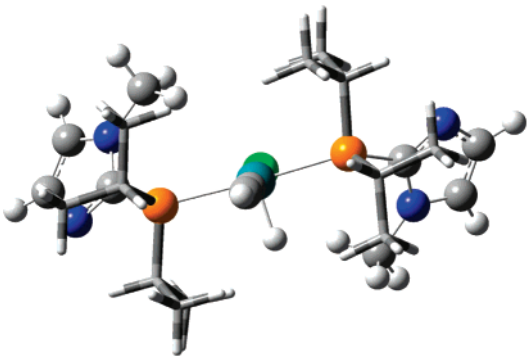

Figure 5. BDMM-optimized geometry of **4e-HCCH**, viewed roughly along the RhCC axis, showing the approximate C_2 symmetry.

ates in which the imidazole nitrogen(s) could be acting as internal base revealed that none of these conformers were more stable than the ones just described and shown in Figure 4. In the subsequent BDMM calculations, the *i*-Pr groups were found to be most stable in a pseudo-C_2 conformation, as shown for compound **4e-HCCH** in Figure 5.

Potential Energy Surface. The relaxed potential energy surface (PES) of the unsubstituted $[RhCl(PH_3)_2](C_2H_2)$ system was determined at the B3LYP/LANL2DZ level in order to investigate the possibility that unanticipated intermediates might contribute to the observed reaction kinetics. To our knowledge, the previous computational studies[41,43,83] did not make a scan of the entire PES. The surface was parametrized as a function of the C2−C1−H and Rh−C1−C2 bond angles, which unambiguously distinguish between **2f**, **4f**, and **5f**, as shown in Figure 6. However, the values of these two bond angles are similar for the hydrido(alkynyl) **4f** and for the η^2-(C,H) alkyne complex **3f**, and this two-dimensional PES is supplemented by an additional scan of the C1−Rh−H bond angle near the **4f** geometry in Figure 6. One species not previously identified to our knowledge is the η^2-(C,C) vinylidene complex seen at the left of Figure 6. Because the geometries of this central framework are not greatly changed upon substitution by the $(i\text{-Pr})_2PR^1$ ligands, the characteristic geometries of the stationary

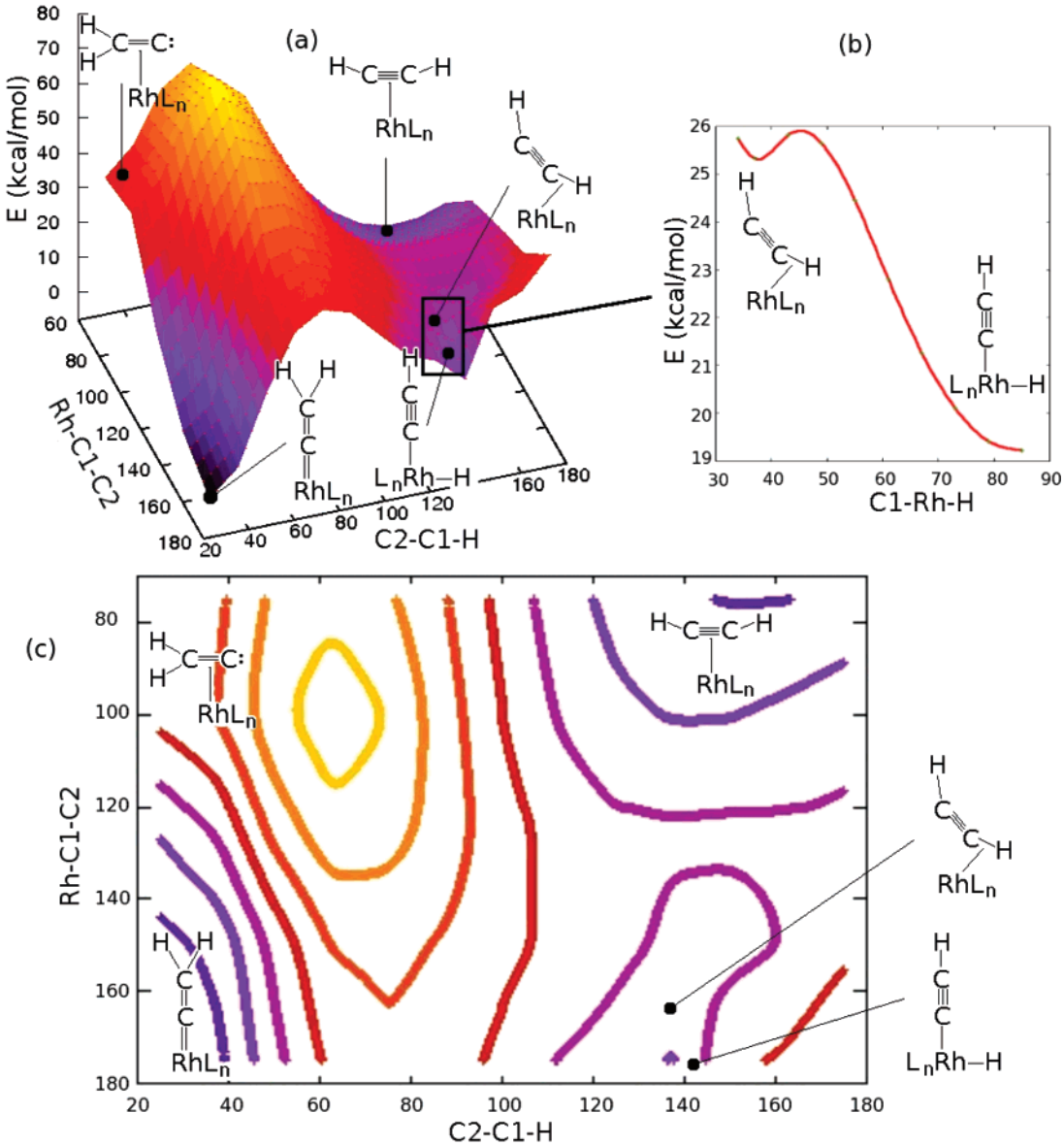

Figure 6. B3LYP/LANL2DZ relaxed PES of the $[RhCl(PH_3)_2](HCCH)$ reaction system, with energies relative to that of **5f**: (a) the smoothed surface as a function of Rh−C1−C2 and C2−C2−H angles; (b) graph of the potential energy as a function of the C1−Rh−H angle near the geometries of **3f** and **4f**, resolving the barrier between them; (c) contour plot of the surface in (a) with contours every 10 kcal mol^{-1}.

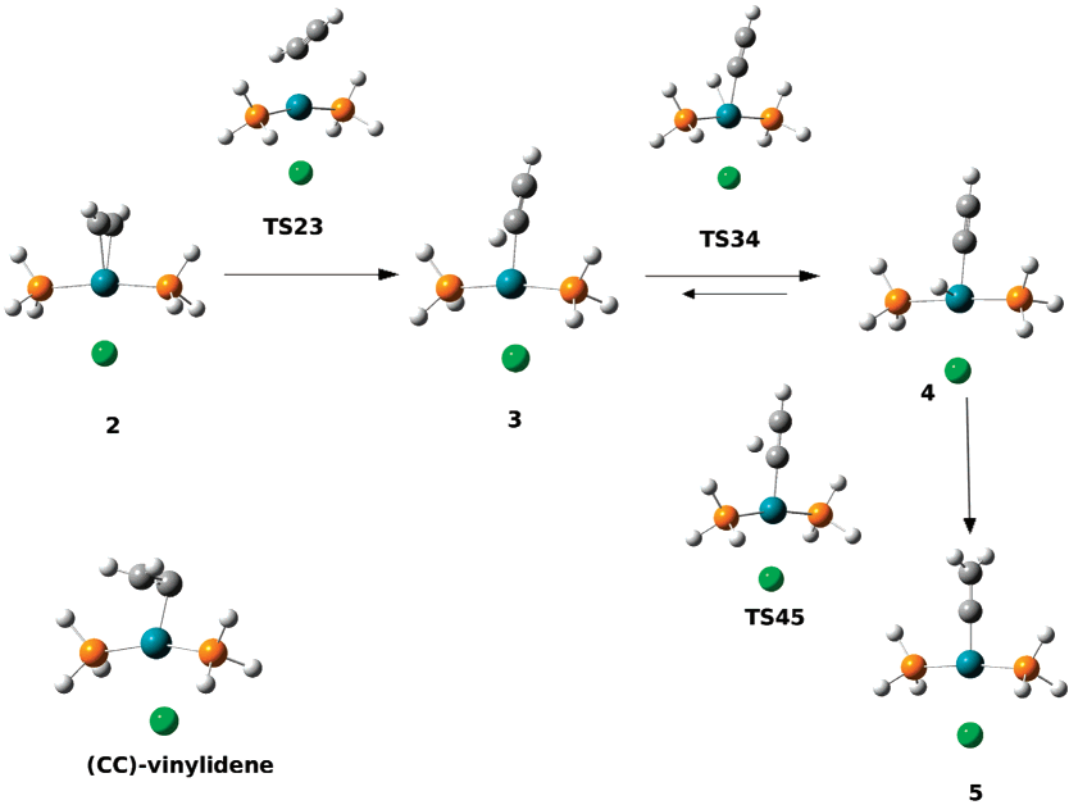

Figure 7. B3LYP/LANL2DZ-optimized critical point geometries for species on the surface shown in Figure 6.

point geometries are shown for the simpler PH_3 ligands in this series of calculations in Figure 7.

The rather surprising stability of the η^2-(C,C) vinylidene complex suggested the possibility of a kinetic contribution from a triplet-spin surface, a situation that to our knowledge has not been considered previously. To test this, the geometries of the alkyne π-complex **2f**, hydrido(alkynyl) species **4f**, the "normal" Rh═C═CH_2 complex **5f**, and its η^2-(C,C) vinylidene isomer were all optimized in their triplet-spin states at the B3LYP/LANL2DZ level, using the unsubstituted model species. The triplet alkyne complex and vinylidene were both found to lie at energies only 33−35 kcal/mol above the singlet vinylidene and 10 kcal mol^{-1} more stable than **TS45**, whereupon a search was made for low-lying triplet geometries with the C2−C1−H bond angle fixed to 69°, its value in the singlet transition states. No points were found that suggested a lower energy path existed between reactant and product along the triplet surface, so these possible structures were not considered further.

Kinetics Analysis. The η^2-(C,H) complex **3** was not identified in the previous study by Wakatsuki et al.,[41] who instead obtained the hydrido(alkynyl) structure **4** with a C−Rh−H bond angle of 69.5° and Rh−H bond length of 1.50 Å. In marked contrast, the recent DFT study by Suresh et al. found the η^2-(C,H) alkyne complex **3** to be an intermediate in the hydrogen shifts to and from the metal center.[43] The present calculations similarly find both **4** (C−Rh−H angle of 86−91°, Rh−H bond length 1.52 Å) and the η^2-(C,H) alkyne complex **3** (C−Rh−H = 38−39°, Rh−H = 1.67−1.71 Å) to be distinct local minima on the PES of each compound studied [H_2PR^1 and $(i\text{-Pr})_2PR^1$ for R^1 = *i*-Pr, Ph, Im, *o*-Tol]. Complex **3** is positioned geometrically between the three other species (**2**, **4**, **5**) in the reaction system such that it appears along each minimum energy pathway connecting the other three species on the PES. However, its impact on the kinetics appears to be negligible, because the hydrido(alkynyl) species **4** is lower in energy and separated from **3** by an energy barrier of only 0.6 kcal/mol in the case of B3LYP/LANL2DZ calculations for $[RhCl(PH_3)_2](C_2H_2)$. Under these conditions, **3** and **4** are subject to a fast equilibrium. Although **4** is not directly coupled to **5** by the minimum energy path, the fast equilibrium approximation allows the integrated rate law for production of vinylidene to be written roughly as [vinylidene] = $[\text{hydride}]_0\{(1 - e^{-at}) - [a(e^{-k_{2-4}t} - e^{-at})/(a - k_{2-4})]\}$, where $a = k_{4-5}/(1 + K_{3-4})$. In the limit that the fast equilibrium constant $K_{3-4} \gg 1$, this equation predicts kinetics consistent with the reaction sequence π-complex $\xrightarrow{k_{2-4}}$ hydride $\xrightarrow{k_{4-5}/K_{3-4}}$ vinylidene. The 1,3-shift required for one-step conversion of **4** to **5** therefore remains, effectively, the mechanism for the reaction. The relaxed PES establishes that a 1,2-shift *does not take place* (along a minimum energy path) directly from **2**, because decreasing the C2−C1−H angle, to place the H atom above the π-bond, causes the energy barrier along the Rh−C1−C2 angle to disappear. Once one H atom moves significantly from one end of the acetylene toward the other, the carbon atom to which it was bound falls toward the Rh atom.

The PES does reveal that the η^2-(C,C) vinylidene species (at Rh−C1−C2 = 79.6°, C2−C1−H = 25.6°) is also a stable geometry in the model species, with a barrier of only about 4 kcal/mol to formation of the product vinylidene. However, no realistic mechanism to reach the η^2-(C,C) vinylidene was identified, and therefore this species was not studied further.

Given that the experimental observations on **2b** show reactions near completion after 1 h at −20 °C, a maximum value of 3600 s may safely be assumed for the half-life of the hydrido(alkynyl) complex at this temperature, corresponding to a minimum rate constant k_{4-5} of 2×10^{-4} s^{-1}. Assuming a typical Arrhenius pre-exponential factor of 10^{12} s^{-1}, which can be estimated from published studies of C−H activation via alkane

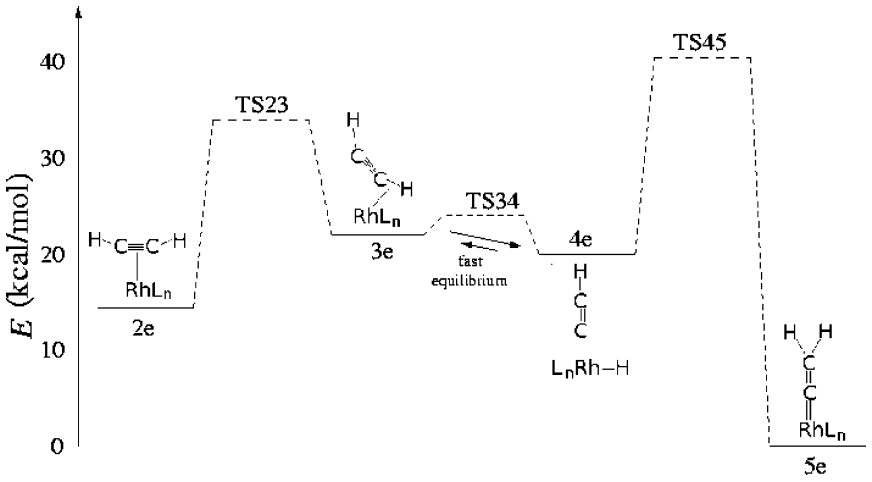

Figure 8. Reaction diagram for $[RhCl(Pi\text{-}Pr_2Im)_2]C_2H_2$ determined at the BDMM level.

Table 3. BDMM-Computed Relative Energies (kcal mol^{-1}) along the Reaction Connecting 2 and 5 in Scheme 2

R^1	ΔE_{2-4}	$E_{a,2-3}$	ΔE_{3-4}	ΔE_{4-5}	E_{a4-5}	ΔE_{2-5}
i-Pr (**a**)	3.4	16.1	3.8	−20.9	21.9	−17.5
Im (**e**)	7.8	18.5	2.2	−22.2	18.3	−14.4
Ph (**c**)	5.9	18.0	3.7	−21.1	20.3	−15.1
o-Tol (**d**)	7.8	19.0	1.9	−22.7	18.5	−14.9

[a] Reference 41.

Table 4. Computed Free Energies of Activation and Rate Constants at −20 °C[a]

R^1	$\Delta G_{a,24}$ (kcal mol^{-1})	k_{2-4} (min^{-1})	$\Delta G_{a,45}$ (kcal mol^{-1})	k_{4-5} (min^{-1})	$k_{2-5,obs}$ (min^{-1})
i-Pr (**a**)	13.9	4.8	19.6	5.7×10^{-5}	nd
Im (**e**)	15.5	0.21	16.7	0.019	0.033
Ph (**c**)	15.8	0.11	17.9	0.0019	0.0035
o-Tol (**d**)	16.5	0.027	15.1	0.45	na

[a] Energies from BDDM calculations, with thermal and zero-point corrections estimated from B3LYP/LANL2DZ calculations on the $[RhCl(H_2PR^1)_2](C_2H_2)$-derived species.

complexes,[84,85] the maximum activation energy should be 21 kcal/mol. The predicted kinetics are highly sensitive to both computational method and basis set among those investigated in this work. However, qualitatively accurate results are obtained using the BDMM-predicted relative energies, presented in Table 3. The reaction diagram based on these values is illustrated for $[RhCl(Pi\text{-}Pr_2Im)_2]C_2H_2$ in Figure 8.

These computational results are consistent with the inability of the NMR studies to detect the hydrido(alkynyl) intermediate **4**. The net reaction is irreversible, because the barrier from vinylidene **5** to **4** is in all cases predicted to be greater than 39 kcal mol^{-1}. In contrast, the first step of the reaction has a reverse barrier about 7 kcal mol^{-1} lower than the **TS45** energy, allowing **4** and π-complex **2** to remain in partial equilibrium during the reaction, with an equilibrium constant less than 10^{-4}. At any time during the reaction, the concentration of the hydrido(alkynyl) complex is therefore expected to be insubstantial compared to that of the π-complex.

Table 4 gives the rate constants for steps 2 and 3 of the reaction (**2** → **4** and **4** → **5**), estimated from elementary transition state theory for the unimolecular case, $k = (k_BT/h)\exp[-\Delta G^{\ddagger}/(RT)]$. For the two ligands for which the rate constant k_{2-5} is measured, the computations predict the k_{4-5} value to be limiting for the formation of vinylidene. The predicted k_{4-5} values each lie within a factor of 2 of the observed rate constants, and the 9.6 factor increase for Im over Ph is predicted to within 10%. The excellent agreement between the observed rate constants and the predicted rate constants for the rate-limiting **4** → **5** step is partly fortuitous, as discussed below. Nonetheless, the successful prediction of the factor of 10 increase in reaction rate from Ph to Im is hoped to be an indication of the value of calculations on systems of this type.

Empirically, the computations indicate that the observed increase in reaction rate with the monoaryl-substituted ligands may be ascribed to an accompanying stabilization of the reaction surface relative to the hydrido(alkynyl) species **4**. The values of ΔE_{2-4}, ΔE_{3-4}, E_{a4-5}, and ΔE_{4-5} in Table 3 show that replacement of one *i*-Pr group by Ph in each ligand raises the energy of **4c** relative to species **2c** and **TS45c** by about 2 kcal mol^{-1}, although this effect is absent when considering **3c** and **5c**. More striking is the effect of substitution by Im or *o*-Tol, which raises the energy of **4e** and **4d** relative to all the other species (**2**, **3**, **5**, and the two transition states) by 1.3 to 4.4 kcal mol^{-1}. The transition state for the **2** → **4** step lies closer in geometry to **4** than to **2**, and its relative energy follows the same trends as **4**. As a consequence, the barrier to the **2** → **4** reaction step increases as the ligands progress in the series *i*-Pr, Ph, Im, *o*-Tol, while the barrier to the **4** → **5** reaction step decreases. Because the **4** → **5** step is the rate-limiting step in all but the *o*-Tol case, the reaction rate increases along this series.

The physical basis for the relative stability of **TS45** with the monoaryl ligands is more elusive. The hydrido(alkynyl) complex is distinct from the other stationary points on the reaction surface in representing the Rh(III) oxidation state with square-pyramidal coordination rather than Rh(I) with square-planar coordination. The shift observed in the CO stretching frequency from R^1 = *i*-Pr to *o*-Tol (Table 1) is consistent with the $(i\text{-Pr})_3P$ ligand contributing a slight destabilization to the CO bond, and the NMR coupling constant data available in Table 2 for **2a**−**2c** and **5a**−**5c** suggest that this effect is also felt in the C_2H_2 and CCH_2 analogues. This interpretation of the spectroscopic evidence is supported by small differences observable in the Rh−C and C−C bond lengths in the optimized BDMM geometries, as listed in Table 5. The Rh−C distance in the π-complex **2a** is 0.008 to 0.012 Å shorter than that in **2b**, **2c**, and **2d**, and the Rh−C1 distance in **TS45a** is 0.009 to 0.011 Å shorter than with the other ligands studied. In contrast, the C−C bond lengths are longer by 0.001 to 0.005 Å in **2a**, **TS45a**, and

(84) Lian, T.; Bromberg, S. E.; Yang, H.; Proulx, G.; Bergman, R. G.; Harris, C. B. *J. Am. Chem. Soc.* **1996**, *118*, 3769−3770.
(85) Northcutt, T. O.; Wick, D. D.; Vetter, A. J.; Jones, W. D. *J. Am. Chem. Soc.* **2001**, *123*, 7257−7270.

Table 5. Comparison of Selected BDMM-Optimized Bond Lengths (Å) or Angles (deg) and Relevant Experimental NMR Data (*J* values, Hz)

	a	b/e	c	d	j[a]
			2		
Rh−C	2.136	2.148	2.146	2.144	2.134
C−C	1.272	1.270	1.271	1.271	1.270
C−C−H	151.8	152.7	152.8	152.7	153.9
$^1J_{C-Rh}$	16.0	14.7	15.3	nd	nd
$^1J_{C-C}$	114.6	115.8	116.2	nd	nd
			3		
Rh−C	2.014	2.023	2.019	2.020	1.990
C−C	1.244	1.243	1.244	1.244	1.241
C−H	1.276	1.246	1.251	1.252	1.332
Rh−H	1.673	1.709	1.704	1.699	1.664
			4		
Rh−C	1.977	1.980	1.985	1.982	1.969
C−C	1.239	1.238	1.239	1.239	1.236
			TS45		
Rh−C	1.929	1.940	1.939	1.938	1.933
C−C	1.278	1.273	1.277	1.277	1.272
			5		
Rh−C	1.833	1.837	1.837	1.836	1.842
C−C	1.330	1.327	1.328	1.328	1.326
$^1J_{C-Rh}$	57.0	55.4	55.6	nd	nd
$^1J_{C-C}$	57.0	58.0	58.7	nd	nd

[a] Results of full basis-set calculations.

5a than when the monoaryl ligands are used. Both effects are consistent with the (*i*-Pr)$_3$P ligand encouraging back-bonding from the metal into a π-antibonding orbital of the C−C bond, strengthening the Rh−C bond while weakening the C−C bond. The weakened C−C bond raises the energy of the complex at these geometries with (*i*-Pr)$_3$P. However, this difference between the ligands is reduced at the hydrido(alkynyl) geometry **4**, where the C−C bond lengths lie within 0.001 Å of each other for all four ligands, and **4a** therefore does not experience the same destabilization as **TS45**, relative to the other ligands. Consequently, the energy difference between **TS45** and **4**, the barrier for the rate-determining step, is lower for the monoaryl ligands as a group, and this accounts for the observed rate difference. The importance of back-bonding in determining the comparative energies is consistent with the conclusions of Suresh et al. in their recent analysis of the alkyne-dependence of this reaction.[43] Contributions of steric effects may also be considered. Looking at calculated geometrical parameters in Table 5, among monoaryl ligands, the Im and *o*-Tol ligands seem indistinguishable from the Ph analogue. In contrast, looking at computed energies and considering the faster observed rate of reaction using **1b** compared with **1c**, it appears that the overall conversion of **2** to **5** is more favorable using the bulkier ligands **1e** and **1d** and that both ΔE_{4-5} and E_{a4-5} are reduced when the bulkier ligands are employed. Here it may be useful to consider the relief of interligand steric interactions on going from five-coordinate intermediate **4** to four-coordinate product **5**.

Because the BDMM calculations treat the two *i*-Pr groups in (*i*-Pr)$_2$PR^1 by molecular mechanics, the effect of these substituents on back-bonding will be underestimated. Partial optimizations (with constrained *i*-Pr dihedral angles) of **4a** and **TS45a** using a full 6-31+G(d,p) basis in place of the crude MM model predict the activation barrier to be nearly 6 kcal mol^{-1} higher than the value in Table 4. These calculations remain too resource-intensive for routine use, however, and the present BDMM calculations appear to provide a useful balance of accuracy and efficiency.

In view of the qualitative success of the present computational work, exploratory calculations were carried out on the same reaction system using triphenylphosphine ligands, derivatives of which have been used recently in catalytic transformations for organic synthesis.[13] In order to adequately represent the electronic structure of the phenyl groups, which was neglected for the *i*-Pr groups in our BDMM calculations, optimizations of **2**−**5** and partial optimizations near the anticipated **TS23** and **TS45** geometries were carried out at the BLYP level using the DQZ,6-31+G(d,p) basis, without molecular mechanics. The limiting step is again predicted to be the hydride-to-vinylidene H-shift. The estimated activation barrier for the Ph$_3$P system **4j** converting to **5j** lies roughly 4 kcal mol^{-1} lower than that for the (*i*-Pr)$_3$P analogue **4a** converting to **5a** (calculated at the same level of theory). This suggests that, like the heterocyclic ligand in the present work, triphenylphosphine ligands such as those used recently for catalytic reactions[13] will contribute a substantial enhancement of the reaction rate over that using (*i*-Pr)$_3$P.

Conclusions

Whereas alkyne transformation on CpRu−bis(phosphine) systems is very strongly influenced and accelerated by heterocyclic groups on the phosphines,[31−33] in the present case the most profound effect of the basic imidazole nitrogen in ligand **1b** appears to be in forming alkyne-free Rh(I) precursor **8** with a labile P,N chelate. In contrast, (*i*-Pr)$_2$PPh (**1c**) appears to form a normal dimer with [Rh$_2$Cl$_2$] core, whereas its *o*-Tol analogue (*i*-Pr)$_2$P(*o*-Tol) (**1d**) suffers metalation of the methyl group on the aromatic ring, unlike the methyl group of **1b**. The effects of phosphine substituent R in (*i*-Pr)$_2$PR on bonding in complexes of CO, HCCH, and its isomer CCH$_2$ could be evaluated using a combination of conventional (e.g., Rh−CO infrared absorption data for **6**) and nontraditional means (particularly ^{13}C−^{13}C coupling data in **2a**−**c** and **5a**−**c** derived from H^{13}C^{13}CH), leading to a consistent picture: the electronic effects of (*i*-Pr)$_2$R (R = Ph, Im′) were similar and different from those of (*i*-Pr)$_3$P.

Qualitatively, ligand **1b** led to much faster formation of vinylidene complex **5** than did **1a**, whereas model ligand **1c** was intermediate in its effects. Alkyne complexes **2** could be formed from **1b** and **1c** below room temperature, but kinetics experiments could not shed light on the molecularity of the conversion of **2** to **5**, nor on the microscopic rate constant for conversion of hydrido(alkynyl) complex **4** to final product. However, lack of isotopic scrambling in double-crossover experiments is significant experimental evidence against alkyne activation on Rh(I) and transformation to vinylidene by way of binuclear species.

These results motivated a computational search of the potential energy surface for alkyne-to-vinylidene transformation on *trans*-(Cl)(R$_2$PR^1)Rh, which revealed an η^2-(C,H) complex, **3**, not far above hydrido(alkynyl) isomer **4**. The magnitudes and trends in the observed rate constants are predicted well by DFT computations using the RCEP core potential and basis of Stevens et al. for the rhodium atom and incorporating the *i*-Pr groups, using a combination of molecular mechanics and DFT. These methods in conjunction with careful surveying of the reaction surface appear to offer tractable and accurate means for modeling reaction dynamics in these and similar studies of C−H activation, catalysis, and transformations useful for organic synthesis.

Experimental Section

General Procedures. All manipulations were carried out in a nitrogen-filled glovebox or using Schlenk techniques. The starting

Table 6. Collection Data for Crystal Structures of the Complexes

	6b	6c	6d	8
formula	$C_{29}H_{54}ClN_4OP_2Rh$	$C_{25}H_{38}ClOP_2Rh$	$C_{27}H_{42}ClOP_2Rh$	$C_{41}H_{46}ClN_4OP_2Rh$
MW	675.06	554.85	582.91	811.12
cryst system	monoclinic	monoclinic	monoclinic	monoclinic
space group	$P2_1/n$	$P2_1/n$	$P2_1/c$	$P2_1/n$
color, habit	yellow block	yellow blade	yellow blade	colorless needle
a [Å]	7.9000(4)	8.5410(8)	10.232(11)	9.6038(6)
b [Å]	24.4193(12)	7.7860(7)	15.409(17)	10.5140(6)
c [Å]	8.9974(4)	19.8080(17)	9.569(10)	19.1961(12)
β [deg]	96.793(1)	96.300(2)	113.509(15)	103.768(1)
V [Å^3]	1723.53(14)	1309.3(2)	1383(3)	1882.6(2)
Z	2	2	2	2
D_{calcd} [g cm^{-3}]	1.301	1.407	1.399	1.431
T [K]	100	208	208	100
$2\theta_{max}$ [deg]	55.0	50.0	52.0	55.0
no. of measd reflns	10 730	7073	8269	11 589
no. of indep reflns	3928	2314	2714	4284
no. of params	195	146	151	241
$R(F)$ ($I > 2\sigma(I)$), %[a]	3.62	4.96	4.75	3.10
$R(wF^2)$ ($I > 2\sigma(I)$), %[b]	8.72	5.31	11.19	8.56
GOF	1.137	1.210	1.089	1.061
res electron density	0.488	0.928	0.712	0.536

[a] $R = \sum||F_o| - |F_c||/\sum|F_o|$. [b] $R(wF^2) = \{\sum[w(F_o^2 - F_c^2)^2]/\sum[w(F_o^2)^2]\}^{1/2}$; $w = 1/[\sigma^2(F_o^2) + (aP)^2 + bP]$, $P = [2F_c^2 + \max(F_o,0)]/3$.

materials [(μ-Cl)Rh(cyclooctene)$_2$]$_2$[86] and [RhCl((*i*-Pr)$_2$PPh)$_2$]$_2$ (**7c**)[55] were prepared as described in the literature. Phosphine ligand **1b** was made as recently described.[87] Acetylene gas (HCCH) from a cylinder containing acetone was passed through concentrated sulfuric acid, then KOH pellets, then powdered K_2CO_3. Labeled derivatives H−^{13}C^{13}C−H (99% ^{13}C, >98% chemical purity) and D-^{13}C^{13}C−D (99% ^{13}C and 98% D, >98% chemical purity) were used as received from Cambridge Isotope Labs (CIL). Care was taken not to pressurize acetylene because of its potentially explosive nature. Benzene, toluene, dichloromethane, hexane, and pentane were distilled from calcium hydride under nitrogen, whereas THF and diethyl ether were distilled from sodium and benzophenone. Acetone, ethyl alcohol, and H_2O were deoxygenated prior to use by nitrogen for 30 min. C_6D_6 and $CDCl_3$ were purchased from CIL, dried over calcium hydride, and vacuum transferred prior to use. Nitrogen was bubbled through samples of CD_2Cl_2, THF-d_8, and toluene-d_8 from CIL before use. NMR tubes were silanized by boiling hexamethyldisilazane in the tube for about a minute, followed by rinsing the cooled tube with pentane and heating the tube under vacuum before filling it with nitrogen. Unless noted otherwise, ^{1}H NMR spectra were obtained on either a Varian Gemini 200 MHz spectrometer or Varian Inova 500 MHz spectrometer. ^{13}C NMR spectra were obtained at 125.7 MHz on a Varian Inova 500 MHz instrument. Both ^{1}H NMR and ^{13}C NMR chemical shifts were reported in parts per million downfield from tetramethylsilane and referenced to the solvent resonances (^{1}H NMR: 7.16 ppm for C_6HD_5, 7.27 ppm for $CHCl_3$, 5.28 ppm for $CHDCl_2$; ^{13}C NMR: 128.39 ppm for C_6D_6, 77.23 ppm for $CDCl_3$, and 54.00 ppm for CD_2Cl_2), where ^{1}H NMR chemical shifts are followed by multiplicity, coupling constants J in hertz, and integration in parentheses. The values for coupling constants in the AA′XX′ systems of H^{13}C^{13}CH complexes were determined using guidance from the literature[88,89] and simulation of spectra using the program WINDNMR. ^{31}P NMR spectra were obtained at 80.95 MHz on the Gemini or at 202.374 MHz on the Inova, and chemical shifts were referenced to external 85% H_3PO_4(aq). Deuterium NMR experiments were run at JEOL USA by Dr. Ashok Krishnaswami using an ECA-500 spectrometer. Elemental analyses were performed at NuMega Resonance Labs, San Diego, CA.

Data relating to the X-ray structural determinations are collected in Table 6. All data were collected on Bruker diffractometers equipped with APEX CCD detectors. All structures were solved by direct methods and refined with anisotropic thermal parameters and idealized hydrogen atoms. All software is contained in the SMART, SAINT, and SHEXTL libraries distributed by Bruker-AXS (Madison, WI). Complete disclosures about the crystallographic work may be found in the deposited CIF files.

Preparation of 6b. In the glovebox, a mixture was made in a test tube using [Rh(μ-Cl)(cyclooctene)$_2$]$_2$ (116.0 mg, 0.16 mmol) and dry C_6H_6 (3 mL). Carbon monoxide was bubbled through the mixture for 1 min, until the color of the solution lightened to yellow. A solution of **1b** (163.2 mg, 0.64 mmol) in dry C_6H_6 (3 mL) was added. After 10 min the yellow solution was concentrated *in vacuo* to 0.5 mL and pentane (3 mL) was added. The complex precipitated directly. Removing the supernatant with a pipet and washing with pentane (2 mL) followed by drying *in vacuo* resulted in a pure pale yellow powder (193.8 mg, 90%). ^{1}H NMR ($CDCl_3$, 500 MHz): δ 6.71 (s, 2H, imidazole H-4), 4.12 (s, 6H, N-CH_3), 3.00−3.10 (m, 4H, Me_2CH−), 1.28 (dvt, $^3J_{H-H}$ = 7.0 Hz, N = 14.5 Hz, 12H, $(CH_3)_2$CH−), 1.26 (s, *t*-Bu, 18H), 1.17 (dvt, $^3J_{H-H}$ = 7.0 Hz, N = 17.5 Hz, 12H, $(CH_3)_2$CH−). ^{31}P NMR ($CDCl_3$, 80.95 MHz): δ 25.8 (d, $^1J_{P-Rh}$ = 118.5 Hz). ^{13}C NMR ($CDCl_3$, 125.7 MHz): δ 186.39 (d, $^1J_{C-Rh}$ = 73.6 Hz, $^2J_{C-P}$ = 15.5 Hz), 153.3 (vt, N = 8.3 Hz), 137.7 (vt, N = 62.1 Hz), 118.5 (s), 36.3 (s), 32.0 (s), 30.3 (s), 24.9 (vt, N = 28.3 Hz), 19.5 (vt, N = 5.3 Hz), 18.7 (s). IR ($CDCl_3$, NaCl): ν_{CO} 1968.2 cm^{-1}. Anal. Calcd for $C_{29}H_{54}ClN_4OP_2Rh$ (675.07): C, 51.60; H, 8.06; N, 8.30. Found: C, 51.20; H, 7.83; N, 8.28.

Diffusion of a small fraction from toluene−petroleum ether resulted in yellow crystals suitable for crystal structure determination.

Synthesis of 6c. In the glovebox, a vial was charged with a stir bar and [Rh(μ-Cl)(cyclooctene)$_2$]$_2$ (33.4 mg, 0.0465 mmol) and CH_2Cl_2 (2 mL). Outside the glovebox, CO was bubbled through the mixture for ca. 30 s, and the cap was closed quickly. The solution lightened in color. The vial was brought into the glovebox and (*i*-Pr)$_2$PPh (37.9 mg, 0.195 mmol) was added using CH_2Cl_2 (total 5 mL, in portions). After 1 h, the solution was concentrated and the residue crystallized from THF (ca. 3 mL) initially warmed, into which was allowed to diffuse petroleum ether for 1 day. After this time some crystals had formed but significant color remained in

(86) van der Ent, A.; Onderdelinden, A. L. *Inorg. Synth.* **1973**, *14*, 92−95.

(87) Grotjahn, D. B.; Gong, Y.; Zakharov, L. N.; Golen, J. A.; Rheingold, A. L. *J. Am. Chem. Soc.* **2006**, *128*, 438−453.

(88) Pople, J. A.; Schneider, W. G.; Bernstein, H. J. *High-resolution Nuclear Magnetic Resonance*; McGraw-Hill: New York, 1959.

(89) Günther, H. *Angew. Chem., Int. Ed. Engl.* **1972**, *11*, 861−874.

the liquid, so petroleum ether was added to the mixture and the vial stored at −40 °C for 2 days. The cold supernatant was removed by pipet and the yellowish crystals stored under vacuum to yield **6c** (46.0 mg, 89%). ^{1}H NMR ($CDCl_3$, 500 MHz): δ 7.76−7.82 (m, 4H), 7.42−7.46 (m, 6H), 2.95 (septet of vt, $^3J_{H-H}$ = 7.0 Hz, *N* = 6.0 Hz, 4H), 1.29 (dvt, $^3J_{H-H}$ = 7.0 Hz, *N* = 17.0 Hz, 12H), 1.13 (dvt, $^3J_{H-H}$ = 7.0 Hz, *N* = 14.0 Hz, 12H). ^{13}C{^{1}H} NMR ($CDCl_3$, 125.7 MHz): δ 187.3 (dt, J_{C-Rh} = 73.6 Hz, J_{C-P} = 15.3 Hz), 134.9 (vt, *N* = 10.6 Hz), 130.2 (s), 129.3 (dvt, J_{C-Rh} = 1.8 Hz, *N* = 35.4 Hz), 127.7 (vt, *N* = 9.7 Hz), 29.9 (s), 22.2 (vt, *N* = 23.9 Hz), 19.2 (vt, *N* = 5.5 Hz), 18.2 ppm (s). ^{31}P{^{1}H} NMR ($CDCl_3$, 80.95 MHz): δ 42.6 ppm (d, $^1J_{P-Rh}$ = 124.4 Hz). Anal. Calcd for $C_{25}H_{38}ClOP_2Rh$ (554.87): C, 54.11; H, 6.90. Found: C, 54.38; H, 6.78.

Crystals suitable for X-ray diffraction were found in the bulk sample crystallized from THF−petroleum ether.

Synthesis of 6d. By a procedure similar to that used to make **6c**, [Rh(μ-Cl)(cyclooctene)$_2$]$_2$ (35.7 mg, 0.0497 mmol) and (*i*-Pr)$_2$P-(o-tol) (43.5 mg, 0.209 mmol) gave **6d** (52.7 mg, 91%). ^{1}H NMR ($CDCl_3$, 500 MHz): δ 7.42−7.47 (m, 2H), 7.33 (t, $^3J_{H-H}$ = 7.5 Hz, 2H), 7.27−7.31 (m, 2H), 7.23 (t, $^3J_{H-H}$ = 7.5 Hz, 2H), 3.12 (s, 6H), 2.80−2.95 (br featureless m, 4H), 1.32 (dvt, $^3J_{H-H}$ = 7.5 Hz, *N* = 15.5 Hz, 12H), 1.15 (dvt, $^3J_{H-H}$ = 7.0 Hz, *N* = 14.0 Hz, 12H). ^{13}C{^{1}H} NMR ($CDCl_3$, 125.7 MHz): δ 186.8 (dt, J_{C-Rh} = 74.6 Hz, J_{C-P} = 15.4 Hz), 144.4 (vt, *N* = 13.1 Hz), 132.7 (s), 132.3 (vt, *N* = 7.4 Hz), 129.6 (s), 126.6 (vt, *N* = 33.6 Hz), 124.8 (vt, *N* = 6.0 Hz), 25.3 (vt, *N* = 9.4 Hz), 23.8 (br vt, *N* = ca. 20 Hz), 19.9 (vt, *N* = 5.3 Hz), 18.2 ppm (sl br s). ^{31}P{^{1}H} NMR ($CDCl_3$, 80.95 MHz): δ 31.1 ppm (d, $^1J_{P-Rh}$ = 121.0 Hz). Anal. Calcd for $C_{27}H_{42}ClOP_2Rh$ (582.93): C, 55.63; H, 7.26. Found: C, 55.51; H, 6.88.

Crystals suitable for X-ray diffraction were found in the bulk sample crystallized from THF−petroleum ether.

Preparation of RhCl[(*i*-Pr)$_2$PIm′]$_2$ (8). To a solution of [(μ-Cl)Rh(cyclooctene)$_2$]$_2$ (87.2 mg, 0.122 mmol) in CH_2Cl_2 (10 mL) was added **1b** (123.6 mg, 0.486 mmol). After stirring for 10 min at room temperature, the solvent was evaporated *in vacuo*. The remaining yellow or brownish-yellow solid was washed with three 3 mL portions of hexanes and dried, yield 148.4 mg (95%). ^{1}H NMR (200 MHz, CD_2Cl_2): δ 6.68, 6.49 (both s, 2H, Im′-*H*), 4.53, 3.60 (both s, 6H, N-C*H*$_3$), 2.55, 2.17 (both br, 4H, PC*H*Me$_2$), 1.37, 1.26 (both s, 18H, *t*Bu), 1.43−1.14 (m, 24H, PCHC*H*$_3$). ^{31}P NMR (80.95 MHz, CD_2Cl_2): δ 47.0 (dd, $^1J_{P-Rh}$ = 181.1 Hz, $^2J_{P-P}$ = 42.2 Hz), 30.0 (dd, $^1J_{P-Rh}$ = 162.6 Hz, $^2J_{P-P}$ = 42.7 Hz). ^{13}C NMR (125.7 MHz, CD_2Cl_2): δ 155.0 (dd, $^3J_{C-P}$ = 10.1 Hz, $^5J_{C-P}$ = 6.3 Hz, P-Im′-C4), 151.6 (d, $^3J_{PC}$ = 7.0 Hz, Im′-C4), 149.6 (dd, $^1J_{C-P}$ = 27.8 Hz, $^3J_{C-P}$ = 6.7 Hz, P-Im′-C2), 143.4 (d, $^1J_{C-P}$ = 60.0 Hz, Im′-C2), 117.5, 117.1 (both s, Im′-C5), 36.8, 34.9 (both s, Im′-N-*C*H$_3$), 32.1, 32.0 (both s, Im′-*C*Me$_3$), 30.6, 30.1 (both s, Im′-C(*C*H$_3$)$_3$), 23.7, 23.5 (both s, P*C*HMe$_2$), 20.7, 20.5 (both s, PCH*Me*$_2$), 19.2 (s, PCH(*C*H$_3$)$_2$). Anal. Calcd for $C_{28}H_{54}ClN_4P_2Rh$ (647.06): C, 51.97; H, 8.41; N, 8.66. Found: C, 48.01; H, 7.47; N, 7.73. For $C_{28}H_{54}ClN_4P_2Rh{\cdot}CH_2Cl_2$ (731.99): calcd C, 47.58; H, 7.71; N. 7.65.

Synthesis of 9. The dimer [Rh(μ-Cl)(cyclooctene)$_2$]$_2$ (44.8 mg, 0.0624 mmol) was suspended in pentane (1 mL), and (*i*-Pr)$_2$P(*o*-tol) (53.5 mg, 0.257 mmol) was dissolved in pentane (1 mL). The solution was added to the stirred suspension, and pentane (total 4 mL) was used to rinse the weighing vial. Within 5 min, the solids had dissolved to give an orange solution. After 30 min, the mixture was concentrated. Pentane was added to the red, oily residue and the mixture concentrated. This was repeated. Attempts to crystallize the product did not succeed, and further analysis was performed on the residue (68.8 mg). Anal. Calcd for $C_{26}H_{42}ClP_2Rh$ (554.92): C, 56.27; H, 7.63. Found: C, 54.25; H, 7.74.

^{1}H NMR (CD_2Cl_2, 500 MHz, 30 °C): δ 7.4−7.6 (br featureless m, 2H), 7.1−7.4 (br featureless m, 6H), 2.68−2.82 (br featureless m, 4H), 1.7−2.2 (br featureless m, 2 or 3H), 1.31 (dd, *J* = 7.0, 15.6 Hz, 12H), 1.16 (dd, *J* = 7.0, 13.5 Hz, 12H), −6 to −13 ppm (br featureless peak, 1 or 2H). In addition, minor broad, featureless peaks were seen at 3.90−4.02 (0.15H), 3.56−3.64 (0.12H), and −20 to −22 ppm (ca. 0.2H). Partial spectrum at −30 °C: 7.55 (t, *J* = 7.0 Hz, 1H), 7.42 (t, *J* = 7.0 Hz, 1H), 7.32−7.37 (m, 1H), 7.26−7.32 (m, 2H), 7.18−7.26 (m, 2H), 7.14 (t, *J* = 7.0 Hz, 1H), 1.90 (s, 3H), 1.0−1.3 (m, 24H), −6.0 to −8.5 (br featureless m, 1H), −10 to −13 (br featureless m, 1H). Because the sample was not pure, and some resonances were overlapping, and there were other, minor peaks, it is very likely that even for the major species not all peaks were assigned. ^{31}P{^{1}H} NMR (CD_2Cl_2, 202.374 MHz, 0 °C): δ 72.3 ppm (dd, $^1J_{P-Rh}$ = 119.2 Hz and $^2J_{P-P}$ = 367.5 Hz) and 39.1 ppm (dd, $^1J_{Rh-P}$ = 111.5 Hz and $^2J_{P-P}$ = 367.5 Hz). IR (CH_2Cl_2, NaCl): 2960, 2929, 2872 (m), 2110 (w, sl br).

Preparation of 5c-CCHBu. A solution of [(μ-Cl)Rh(cyclooctene)$_2$]$_2$ (144.5 mg, 0.201 mmol) in C_6H_6 (3 mL) was treated with a solution of (*i*-Pr)$_2$PPh (184.4 mg, 0.949 mmol) in C_6H_6 (3 mL). After stirring for 10 min, 1-hexyne (0.10 mL, 0.872 mmol) was added to the solution via syringe. The reaction was stirred overnight. The solvent was removed *in vacuo*, and the remaining solid was washed three times with portions (3 mL) of pentane. The product was obtained after recrystallizing from pentane at −53 °C as violet crystals, yield 176.6 mg (72%). ^{1}H NMR (500 MHz, $CDCl_3$): δ 7.74−7.69 (m, 4H, Ph), 7.40−7.37 (m, 6H, Ph), 3.03−2.95 (m, 4H, PC*H*Me$_2$), 1.58 (tq, $^5J_{H-P}$ = 2 Hz, $^3J_{H-vinylidene\ H} \approx {}^3J_{H-CH2}$ = 7.7 Hz, 2H, C=CHC*H*$_2$CH$_2$CH$_2$CH$_3$), 1.27 (dvt, $^3J_{H-H}$ = 7 Hz, *N* = 14 Hz, PCHC*H*$_3$), 1.09 (dvt, $^3J_{H-H}$ = 7 Hz, *N* = 14 Hz, PCHC*H*$_3$), 0.73 (∼sextet, $^3J_{H-H} \approx$ 7.5 Hz, 2H, C=CHCH$_2$-CH$_2$C*H*$_2$CH$_3$), 0.56 (t, *J* = 7.0 Hz, 3H, C=CHCH$_2$CH$_2$CH$_2$C*H*$_3$), 0.21 (∼quintet, $^3J_{H-H}$ = 7.5 Hz, 2H, C=CHCH$_2$C*H*$_2$CH$_2$CH$_3$), 0.00 (dtt, $^3J_{H-Rh}$ = 1.8 Hz, $^3J_{H-P}$ = 3.5 Hz, $^3J_{H-CH2}$ = 8 Hz, 1H, Rh=C=C*H*). Assignments of the proton resonances in the vinylidene side chain were made by means of a COSY spectrum. ^{31}P NMR (80.95 MHz, $CDCl_3$): δ 40.1 (d, $^1J_{P-Rh}$ = 142.3 Hz). ^{13}C (125.7 MHz, $CDCl_3$): δ 297.7 (td, $^2J_{C-P}$ = 17.4 Hz, $^1J_{C-Rh}$ = 55.2 Hz, Rh=*C*), 135.0 (vt, *N* = 10.4 Hz, PPh-*meta* or *ortho*), 129.4 (dvt, $^2J_{C-Rh}$ = 2.1 Hz, *N* = 35.6 Hz, PPh-*ipso*), 129.3 (s, PPh-*para*), 127.0 (vt, *N* = 8.7 Hz, PPh-*ortho* or *meta*), 106.1 (td, $^3J_{C-P}$ = 6.9 Hz, $^2J_{C-Rh}$ = 15.1 Hz, Rh=C=*C*), 33.3 (s, C=CHCH$_2$*C*H$_2$CH$_2$-CH$_3$), 21.94 (vt, *N* = 22.8 Hz, P*C*HCH$_3$), 21.93 (s, C=CHCH$_2$-CH$_2$*C*H$_2$CH$_3$), 19.4 (vt, *N* = 5.9 Hz, PCH*C*H$_3$), 18.2 (s, PCH*C*H$_3$), 15.7 (s, C=CH*C*H$_2$CH$_2$CH$_2$CH$_3$), 13.7 (s, C=CHCH$_2$CH$_2$CH$_2$*C*H$_3$). Carbon assignments were made by analogy with assignments made for **5b-CCHBu** using gCOSY, gHMQC, and gHMBC. Anal. Calcd for $C_{30}H_{48}ClP_2Rh$ (609.01): C, 59.17; H 7.94. Found: C, 59.56; H, 7.96.

Preparation of 5b-CCHBu. A solution of [(μ-Cl)Rh(cyclooctene)$_2$]$_2$ (188.3 mg, 0.262 mmol) in C_6H_6 (3 mL) was treated with a solution of **1b** (276.3 mg, 1.09 mmol) in C_6H_6 (3 mL). After stirring for 10 min, 1-hexyne (0.10 mL, 0.872 mmol) was added to the solution via syringe and the reaction was stirred overnight. The solvent was removed *in vacuo*, and the remaining solid was washed three times with portions (3 mL) of pentane. The product was obtained after recrystallizing from pentane at −53 °C as violet crystals, yield 245.4 mg (64%). ^{1}H NMR (500 MHz, $CDCl_3$): δ 6.67 (s, 2H, Im′-H), 3.97 (s, 6H, Im′-NC*H*$_3$), 3.17−3.08 (m, 4H, PC*H*CH$_3$), 1.94 (tq, $^5J_{H-P}$ = 2 Hz, $^3J_{H-vinylidene\ H} \approx {}^3J_{H-CH2}$ = 7.7 Hz, 2H, C=CHC*H*$_2$CH$_2$CH$_2$CH$_3$), 1.26 (s, 18H, Im′-C(C*H*$_3$)$_3$), 1.23, 1.15 (both dvt, $^3J_{H-H}$ = 0.5 *N* = 7.0 Hz, 12H, PCHC*H*$_3$), 1.01 (∼sextet, $^3J_{H-H}$ = 7.5 Hz, 2H, C=CHCH$_2$CH$_2$C*H*$_2$CH$_3$), 0.74 (t, 3H, *J* = 7.5 Hz, C=CHCH$_2$CH$_2$CH$_2$C*H*$_3$), 0.70 (∼quintet, $^3J_{H-H}$ = 7.5 Hz, 2H, C=CHCH$_2$C*H*$_2$CH$_2$CH$_3$), 0.37 (dtt, $^3J_{H-Rh}$ = 1 Hz, $^3J_{H-P}$ = 3.0 Hz, $^3J_{H-CH2}$ = 8 Hz, 1H, Rh=C=C*H*CH$_2$CH$_2$CH$_2$-CH$_3$). ^{31}P NMR (80.95 MHz, $CDCl_3$): δ 23.2 (d, $^1J_{P-Rh}$ = 135.3 Hz). ^{13}C NMR (125.7 MHz, $CDCl_3$): δ 298.0 (td, $^2J_{C-P}$ = 17.4 Hz, $^1J_{C-Rh}$ = 55.2 Hz, Rh=*C*), 152.8 (vt, *N* = 7.7 Hz, Im′-C4),

138.0 (vt, $N = 60.4$ Hz, Im′-C2), 117.7 (s, Im′-C5), 104.9 (td, $^3J_{C-P} = 6.5$ Hz, $^2J_{C-Rh} = 15.5$ Hz, Rh=C=*C*), 36.1 (s, Im′-N-*C*H$_3$), 33.6 (s, C=CHCH$_2$*C*H$_2$CH$_2$CH$_3$), 31.8 (s, Im′-*C*(CH$_3$)$_3$), 30.1 (s, Im′-C(*C*H$_3$)$_3$), 24.0 (vt, $N = 27.3$ Hz, P*C*HCH$_3$), 21.9 (s, C=CHCH$_2$-CH$_2$*C*H$_2$CH$_3$), 19.6 and 18.7 (two sl br s, PCH*C*H$_3$), 14.7 (s, C=CH*C*H$_2$CH$_2$CH$_2$CH$_3$), 13.7 (s, C=CHCH$_2$CH$_2$CH$_2$*C*H$_3$). Proton and carbon assignments were made using gCOSY, gHMQC, and gHMBC. Anal. Calcd for $C_{34}H_{64}ClN_4P_2Rh$ (729.20): C, 56.00; H, 8.85; N, 7.68. Found: C, 56.12; H, 8.73; N, 7.86.

Reaction of [RhCl((*i*-Pr)$_2$PPh)$_2$]$_2$ (7c) with ^{13}C-Labeled Acetylene. A J-Young tube containing a solution of **7c** (10.1 mg, 0.010 mmol) in CD_2Cl_2 (1.0 mL) was stored in the glovebox freezer (−40 °C) for a few minutes before it was removed, and ^{13}C-labeled acetylene H^{13}C≡^{13}CH (2 mL in a syringe) was bubbled slowly for 1 min. The J-Young tube was then sealed and immediately taken out of the glovebox and placed in an acetone−dry ice bath for transport to a precooled (−20 °C) NMR probe. The NMR data were acquired immediately after brief experiment setup. ^{1}H NMR (500 MHz, CD_2Cl_2, −20 °C) for **2c-H^{13}C^{13}CH**: δ 7.58−7.42 (m, 10H, Ph), 3.30 (HH′CC′ 10 peaks with additional coupling $^2J_{H-Rh} = 2.5$ Hz: $^1J_{H-C} = 233.2$ Hz, $^2J_{H-C} = 29.1$ Hz, $^3J_{H-H} = 1.7$ Hz, $^1J_{C-C} = 115.8$ Hz, 2H, Rh-η^2-*H*^{13}C≡^{13}C*H*′), 2.54−2.65 (m, 4H, PC*H*CH$_3$), 1.25 (dvt, $^3J_{H-H} = 0.5\ N = 7.5$ Hz, PCHC*H*$_3$), 1.07 (dvt, $^3J_{H-H} = 0.5\ N = 7.5$ Hz, PCHC*H*$_3$). ^{31}P NMR (202.374 MHz, CD_2Cl_2, −20 °C): δ 35.8 (d, $^1J_{P-Rh} = 120.5$ Hz). Partial ^{13}C NMR (125.7 MHz, CD_2Cl_2, −20 °C): δ 68.7 (dt, $^1J_{C-Rh} = 15.3$ Hz, $^2J_{C-P} = 2.0$ Hz, Rh-(η^2-H^{13}*C*^{13}*C*H)). [In a separate experiment using less alkyne, a sample observed quickly at 30 °C showed peaks centered on 3.25 ppm for the HH′CC′ spin system, $^2J_{H-Rh} = 2.5$ Hz, $^1J_{H-C} = 232.8$ Hz, $^2J_{H-C} = 29.0$ Hz, $^3J_{H-H} = 1.8$ Hz, $^1J_{C-C} = 116.2$ Hz.] The sample was allowed to warm to room temperature. NMR showed conversion of π-complex **2c-H^{13}C^{13}CH** to vinylidene RhCl(P*i*Pr$_2$Ph)$_2$(=^{13}C=^{13}CH$_2$) (**5c-^{13}C^{13}CH$_2$**). ^{1}H NMR (500 MHz, CD_2Cl_2, 30 °C): δ 7.73−7.77 (m, 10H, Ph), 2.94−3.06 (m, 4H, PC*H*CH$_3$), 1.25 (dvt, $^3J_{H-H} = 0.5\ N = 7.8$ Hz, PCHC*H*$_3$), 1.13 (dvt, $^3J_{H-H} = 0.5\ N = 7$ Hz, PCHC*H*$_3$), −0.26 (dtd, $^2J_{H-C} = 3.0$ Hz, $^4J_{H-P} = 3.5$ Hz, $^1J_{H-C} = 163.0$ Hz, 2H, Rh=^{13}C=^{13}C*H*$_2$). ^{31}P NMR (80.95 MHz, CD_2Cl_2, 30 °C): δ 41.6 (ddd, $^1J_{P-Rh} = 142.3$ Hz, $^2J_{P-C} = 17.3$ Hz, $^3J_{P-C} = 6.7$ Hz). Partial ^{13}C NMR (125.7 MHz, CD_2Cl_2, 30 °C): δ 297.9 (tdd, $^2J_{C-P} = 17.1$ Hz, $^1J_{C-Rh} = 55.6$ Hz, $^1J_{C-C} = 58.7$ Hz, Rh=^{13}*C*=^{13}CH$_2$), 90.7 (tdd, $^3J_{C-P} = 6.5$ Hz, $^2J_{C-Rh} = 15.7$ Hz, $^1J_{C-C} = 58.7$ Hz, Rh=^{13}C=^{13}*C*H$_2$).

Reaction of RhCl((*i*-Pr)$_2$PIm′)$_2$ (8) with ^{13}C-Labeled Acetylene. A J-Young tube containing a solution of **8** (12.8 mg, 0.020 mmol) in CD_2Cl_2 (1.0 mL) was stored in the glovebox freezer (−40 °C) for a few minutes before it was removed and ^{13}C-labeled acetylene H^{13}C≡^{13}CH (2 mL in a syringe) was bubbled slowly for 1 min. The J-Young tube was then sealed and immediately taken out of the glovebox and placed in an acetone−dry ice bath for transport to a precooled (−20 °C) NMR probe. The NMR data were acquired immediately after brief experiment setup. ^{1}H NMR (500 MHz, CD_2Cl_2, −20 °C) for **2b-H^{13}C^{13}CH**: δ 6.79 (s, 2 H, Im′-*H*), 4.23 (s, 6 H, Im′ N-C*H*$_3$), 3.78 (HH′CC′ 10 peaks with additional coupling, $^2J_{H-Rh} = 2.4$ Hz; broadness of peaks under these conditions precluded determining the various coupling constants), 2.1−2.8 (featureless m, 6H, PC*H*CH$_3$), 1.38 (s, 18H, Im′-C(C*H*$_3$)$_3$), 0.8−1.4 (featureless m, integral hard to determine accurately, PCHC*H*$_3$). ^{31}P NMR (202.374 MHz, CD_2Cl_2, −20 °C): δ 19.4 (d, $^1J_{P-Rh} = 117.4$ Hz). ^{13}C NMR (125.7 MHz, CD_2Cl_2, −20 °C): δ 152.6 (vt, $N = 7.2$ Hz, Im′ C4), 137.6 (vt, $N = 57.8$ Hz, Im′ C2), 118.1 (s, Im′ C5), 67.5 (dt, $^1J_{C-Rh} = 13.1$ Hz, $^2J_{C-P} = 2.0$ Hz, Rh-(η^2-H^{13}*C*^{13}*C*H)), 37.2 (s, Im′ N-*C*H$_3$), 31.9 (s, *C*(CH$_3$)$_3$), 30.1 (s, C(*C*H$_3$)$_3$), 20−23 (br, *C*H(CH$_3$)$_2$), 17.5−18.8 (br, CH(*C*H$_3$)$_2$)). [In a separate experiment using less alkyne, a sample observed quickly at 20 °C showed peaks centered on 3.69 ppm for the HH′CC′ spin system, $^2J_{H-Rh} = 2.6$ Hz, $^1J_{H-C} = 232.9$ Hz, $^2J_{H-C} = 29.3$ Hz, $^3J_{H-H} = 1.7$ Hz, $^1J_{C-C} = 115.8$ Hz.] After spectra were acquired at low temperature, the sample was allowed to warm to room temperature. NMR showed conversion of π-complex to the corresponding vinylidene RhCl(P*i*Pr$_2$Im′)$_2$(=^{13}C=^{13}CH$_2$) (**5b-^{13}C^{13}CH$_2$**), although the mixture contained minor unidentified species, which made complete spectral assignments difficult. ^{1}H NMR (500 MHz, CD_2Cl_2, 30 °C): δ 6.78 (s, 2H, Im′-H), 3.96 (s, 6H, Im′-NC*H*$_3$), 3.10−3.20 (m, 4H, PC*H*CH$_3$), 1.30 (s, 18H, Im′-C(C*H*$_3$)$_3$), 1.25 (dvt, signal partially hidden by other resonances, 12H, PCHC*H*$_3$), 1.17 (dvt, $^3J_{H-H} = 0.5\ N = 7.0$ Hz, 12H, PCHC*H*$_3$), 0.06 (dtd, $^2J_{H-C} = 3.0$ Hz, $^2J_{H-P} = 3.5$ Hz, $^1J_{H-C} = 163.0$ Hz, 2H, Rh=^{13}C=^{13}C*H*$_2$). ^{31}P NMR (202.374 MHz, CD_2Cl_2, 30 °C): δ 25.7 (ddd, $^3J_{P-C} = 5.9$ Hz, $^2J_{P-C} = 17.0$ Hz, $^1J_{P-Rh} = 135.3$ Hz). Partial ^{13}C NMR (125.7 MHz, CD_2Cl_2, 30 °C): δ 296.7 (tdd, $^2J_{C-P} = 17.1$ Hz, $^1J_{C-Rh} = 55.4$ Hz, $^1J_{C-C} = 58.0$ Hz, Rh=^{13}*C*=^{13}CH$_2$), 89.5 (tdd, $^3J_{C-P} = 5.9$ Hz, $^2J_{C-Rh} = 16.5$ Hz, $^1J_{C-C} = 58.0$ Hz, Rh=^{13}C=^{13}*C*H$_2$).

Kinetics Experiments. All reagents, solvents, NMR tube, and syringes were precooled to −35 °C before any manipulations. Complex **7c** or **8** was dissolved in CD_2Cl_2 (1.00 mL) in a J-Young NMR tube, 1-hexyne was added using a microsyringe, and the NMR tube was then sealed with the screw cap. Quantities used were the following: run 1, complex **8** (13.7 mg, 0.0212 mmol) and 1-hexyne (50 μL, 0.436 mmol, 21.8 equiv); run 2, complex **8** (14.0 mg, 0.0216 mmol) and 1-hexyne (50 μL, 0.436 mmol, 20.2 equiv); run 3, complex **8** (25.7 mg, 0.0397 mmol) and 1-hexyne (50 μL, 0.436 mmol, 11.0 equiv); run 4, complex **8** (37.0 mg, 0.057 mmol) and 1-hexyne (7.0 μL, 0.061 mmol, 1.07 equiv); and finally, run 5, complex **7c** (26.0 mg, 0.0493 mmol) and 1-hexyne (6.0 μL, 0.05 mmol, 1.0 equiv). The tube was immediately removed from the glovebox and placed in an acetone−dry ice bath to prevent the starting of the reaction, and shaken again to obtain a well-mixed solution just before insertion into the NMR probe precooled to −20 °C. The experiment was started immediately afterward, after allowing about 1 min for thermal equilibration and experiment setup. Acquisition parameters included 1 transient of 90° pulse width, followed by acquisition, and then in intervals of between 4 and 10 min between pulses. The data were collected at regular interval times, each one with identical acquisition parameters. The concentration of each component was calculated from the peak intensities of the resonance of each complex against the peak of internal standard (Me$_3$Si)$_4$C, which was set arbitrarily equal to 100.

Crossover Reaction of [RhCl((*i*-Pr)$_2$PPh)$_2$]$_2$ (7c) with 1-Hexyne-1-*d*$_1$ and 3-Methyl-1-butyne. To a NMR tube containing [RhCl((*i*-Pr)$_2$Ph)$_2$]$_2$ (**7c**) (13.2 mg, 0.025 mmol) was added CD_2Cl_2 (0.5 mL). The tube was shaken and sonicated for 2 min to make sure all complex dissolved. The sample was stored at −78 °C in a dry ice−acetone bath. A solution of 1-hexyne-1-*d*$_1$ (2.5 μL, 0.021 mmol) and 3-methyl-1-butyne (2.5 μL, 0.024 mmol) in CD_2Cl_2 (0.5 mL) was added to the NMR tube at −78 °C. The NMR tube was immediately inserted into the precooled NMR probe (−20 °C) after allowing about 2 min for thermal equilibration and experiment setup. The NMR spectra were recorded at three different temperatures: −20, 0, and 30 °C. Spectra at low temperatures (−20 and 0 °C) showed doublets in ^{31}P NMR spectra at δ 32.8 (d, $^1J_{P-Rh} = 123.7$ Hz) and 35.0 (d, $^1J_{P-Rh} = 123.7$ Hz), corresponding to π-complex [RhCl((*i*-Pr)$_2$PPh)$_2$(η^2-CD≡CCH$_2$CH$_2$CH$_2$CH$_3$)] (**2c-DCCBu**) and [RhCl((*i*-Pr)$_2$PPh)$_2$(η^2-CH≡CCH(CH$_3$)$_2$)] (**2c-HC-CiPr**), respectively. After isomerization of π-complex to vinylidene was completed at 30 °C, there were only two doublets, at δ 42.4 (d, $^1J_{P-Rh} = 141.5$ Hz) and 42.1 (d, $^1J_{P-Rh} = 142.7$ Hz), corresponding to the vinylidene [RhCl((*i*-Pr)$_2$PPh)$_2$(=C=CDCH$_2$-CH$_2$CH$_2$CH$_3$)] (**5c-CCDBu**) and [RhCl((*i*-Pr)$_2$PPh)$_2$(=C=CHCH-(CH$_3$)$_2$)] (**5c-CCHiPr**), respectively. ^{1}H NMR spectra indicated no crossover reaction, for **5c-CCDBu**: δ 1.67 (m, Rh=C=CDC*H*$_2$, 2H), 0.78 (m, Rh=C=CDCH$_2$CH$_2$C*H*$_2$CH$_3$, 2H), 0.60 (t, $J = 7.5$ Hz, Rh=C=CDCH$_2$CH$_2$CH$_2$C*H*$_3$, 3H), 0.30 (m, Rh=C=CDCH$_2$-C*H*$_2$CH$_2$CH$_3$, 2H), 0.12 (none, Rh=C=C*D*); for **5c-CCHiPr**: δ

0.05 (d, $^3J_{H-H}$ = 6.5 Hz, Rh=C=CHCH(CH_3)$_2$, 6H), −0.12 (dt, $^3J_{H-H}$ = 10.0 Hz, $^4J_{H-P}$ = 3.5 Hz, Rh=C=C*H*, 1H).

The results from this crossover experiment were compared with those from a similar experiment using an equimolar mixture of undeuterated 1-hexyne and 3-methyl-1-butyne in order to estimate detection limits.

Crossover Reaction of RhCl((*i*-Pr)$_2$PIm′)$_2$ (8) with 1-Hexyne-1-*d*$_1$ and 3-Methyl-1-butyne. To a NMR tube containing RhCl((*i*-Pr)$_2$PIm′)$_2$ (**8**) (13.4 mg, 0.021 mmol) was added CD_2Cl_2 (0.5 mL). The tube was shaken and sonicated for 2 min to make sure all complex dissolved. The sample was then stored at −78 °C in a dry ice−acetone bath. A solution of 1-hexyne-1-*d*$_1$ (1.5 μL, 0.013 mmol) and 3-methyl-1-butyne (1.5 μL, 0.015 mmol) in CD_2Cl_2 (0.5 mL) was added to the NMR tube at −78 °C. The NMR tube was immediately inserted into the precooled NMR probe (−20 °C) after allowing about 2 min for thermal equilibration and experiment setup. The NMR spectra were recorded at three different temperatures: −20, 0, and 30 °C. Interestingly, in ^{31}P NMR spectra at lower temperatures, −20 and 0 °C, for the alkyne π-complexes a broadened peak near 18 ppm was observed, whereas peaks for **8** and final vinylidene complexes were sharp. At 30 °C, the two doublets at δ 25.6 (d, $^1J_{P-Rh}$ = 135.8 Hz) and 25.4 (d, $^1J_{P-Rh}$ = 136.4 Hz) confirmed the formation of vinylidenes [RhCl((*i*-Pr)$_2$PIm′)$_2$(=C=CDCH$_2$CH$_2$CH$_2$CH$_3$)] (**5b-CCDBu**) and [RhCl((*i*-Pr)$_2$PIm′)$_2$(=C=CHCH(CH$_3$)$_2$)] (**5b-CCHiPr**). ^{1}H NMR spectra indicated no crossover reaction, for **5b-CCDBu**: δ 2.04 (m, Rh=C=CDCH_2, 2H), 1.06 (m, Rh=C=CDCH$_2$CH$_2$CH_2CH$_3$, 2H), 0.91 (m, Rh=C=CDCH$_2$CH$_2$CH$_2$CH_3, 3H), 0.77 (m, Rh=C=CDCH$_2$CH_2-CH$_2$CH$_3$, 2H), 0.53 (none, Rh=C=C*D*); for **5b-CCHiPr**: δ 0.48 (d, $^3J_{H-H}$ = 7.0 Hz, Rh=C=CHCH(CH_3)$_2$, 6H), 0.23 (dt, $^3J_{H-H}$ = 10.0 Hz, $^4J_{H-P}$ = 3.0 Hz, Rh=C=C*H*, 1H).

The results from this crossover experiment were compared with those from a similar experiment using an equimolar mixture of undeuterated 1-hexyne and 3-methyl-1-butyne in order to estimate detection limits.

Preparation of π-Complex [RhCl((*i*-Pr)$_3$P)$_2$(η^2-H^{13}C≡^{13}CH)] (2a-H^{13}C^{13}CH) and Isomerization to the Vinylidene. The π-alkyne complex from H^{13}C^{13}CH was prepared in analogy with the method described by Werner et al.[90] A stirred solution of [(μ-Cl)Rh(cyclooctene)$_2$]$_2$ (0.1218 g, 0.170 mmol) in pentane (15 mL) was treated with (*i*-Pr)$_3$P (**1a**) (0.2595 g, 1.62 mmol) and stirred for 20 min at room temperature. The solution was cooled to 0 °C in an ice bath. The acetylene gas (12.5 mL) was bubbled through the solution over 30 s at 1 atm, lightening the reaction mixture color to brownish-yellow. A yellow precipitate began to form. After 10 min the solution was cooled further to −78 °C for 2 h and filtered, and the solid washed with cold (−35 °C) pentane and dried. Yield of **2a-H^{13}C^{13}CH**: 113 mg, 68%.

NMR data for **2a-H^{13}C^{13}CH**: ^{1}H NMR (500 MHz, C_6D_6, 30 °C): δ 3.30 (HH′CC′ 10 peaks with additional coupling, $^2J_{H-Rh}$ = 2.5 Hz, $^1J_{H-C}$ = 228.5 Hz, $^2J_{H-C}$ = 27.5 Hz, $^3J_{H-H}$ = 1.7 Hz, $^1J_{C-C}$ = 114.5 Hz, 2H, Rh-η^2-*H*^{13}C≡^{13}C*H*′), 2.25−2.40 (m, PC*H*, 6H), 1.25 (dvt, $^3J_{H-H}$ = 6.2 Hz, *N* = 13.0 Hz, 36 H, PCHCH_3). ^{1}H NMR (500 MHz, CD_2Cl_2, 30 °C): δ 3.43 (HH′CC′ 10 peaks with additional coupling, $^2J_{H-Rh}$ = 2.5 Hz, $^1J_{H-C}$ = 229.7 Hz, $^2J_{H-C}$ = 28.0 Hz, $^3J_{H-H}$ = 1.7 Hz, $^1J_{C-C}$ = 114.6 Hz, 2H, Rh-η^2-*H*^{13}C≡^{13}C*H*′), 2.34 (septet of vt, *N* = $^3J_{HH}$ = 7.2 Hz, PC*H*, 6H), 1.27 (dvt, $^3J_{H-H}$ = 6.2 Hz, *N* = 13.0 Hz, 36 H, PCHCH_3). ^{31}P NMR (81.0 MHz, C_6D_6, 30 °C): δ 34.4 (td, $^2J_{P-C}$ = 2.4 Hz, $^1J_{P-Rh}$ = 116.5 Hz). ^{13}C NMR (125.7 MHz, C_6D_6, 30 °C): δ 68.9 (td, $^2J_{C-P}$ = 2.4 Hz, $^1J_{C-Rh}$ = 15.7 Hz, H^{13}*C*≡^{13}*C*H), 22.2 (vt, *N* = 17.3, P*C*H), 20.0 (s, PCH*C*H$_3$). ^{13}C NMR (125.7 MHz, CD_2Cl_2, 30 °C): δ 68.4 (td, $^2J_{C-P}$ = 2.4 Hz, $^1J_{C-Rh}$ = 16.0 Hz, H^{13}*C*≡^{13}*C*H), 22.0 (vt, *N* = 17.2, P*C*H), 19.8 (s, PCH*C*H$_3$).

Over 2 days at room temperature the complex formed **5a-^{13}C^{13}CH$_2$**: ^{1}H NMR (500 MHz, C_6D_6, 30 °C): δ 2.78−2.90 (m, PC*H*, 6H), 1.32 (dvt, $^3J_{H-H}$ = 6.0 Hz, *N* = 13.5 Hz, PCHCH_3), −0.13 (qd, $^3J_{H-Rh}$ = $^4J_{H-P}$ = 3.2 Hz, $^1J_{H-C}$ = 161.7 Hz). ^{31}P NMR (80.95 MHz, C_6D_6, 30 °C): δ 42.3 (d, $^1J_{P-Rh}$ = 135.3 Hz). ^{13}C NMR (125.7 MHz, C_6D_6, 30 °C): δ 291.0 (tdd, $^2J_{C-P}$ = 16.0 Hz, $^1J_{C-Rh}$ = $^1J_{C-C}$ = 57.0 Hz, Rh=*C*=^{13}CH$_2$), 89.4 (tdd, $^3J_{C-P}$ = 5.9 Hz, $^2J_{C-Rh}$ = 17.0 Hz, $^1J_{C-C}$ = 56.7 Hz, Rh=^{13}C=^{13}*C*H$_2$). The assignment of $^1J_{C-C}$ reported previously[48] must be incorrect. One interesting comparison regarding this isotopomer and the natural-abundance one is that the magnitude of $^3J_{H-Rh}$ for the ^{1}H resonance at −0.13 ppm is different (3.2 Hz here and 1.0 Hz in the case of **5a-CCH$_2$**).

Preparation of π-Complexes [RhCl((*i*-Pr)$_3$P)$_2$(η^2-HC≡CH)] (2a-HCCH) and [RhCl((*i*-Pr)$_3$P)$_2$(η^2-D^{13}C≡^{13}CD)] (2a-D^{13}C^{13}CD) and Their Isomerization to Vinylidenes. The π-alkyne complex from HCCH was prepared as described by Werner et al.,[90] whereas the labeled one was made using D^{13}C^{13}CD. A stirred solution of [(μ-Cl)Rh(cyclooctene)$_2$]$_2$ (0.232 g, 0.323 mmol) in pentane (30 mL) was treated with (*i*-Pr)$_3$P (**1a**) (0.503 g, 3.14 mmol) and stirred for 10 min at room temperature. The solution was cooled to 0 °C in an ice bath. The acetylene gas (20 mL in the case of D^{13}C^{13}CD) was bubbled through the solution for 10 s at 1 atm, forming instantly a yellow precipitate. The solution was cooled further to −78 °C for 2 h and filtered, and the solid washed with cold (−35 °C) pentane and dried. Yield for **2a-HCCH**: 165.2 mg, 53%; for **2a-D^{13}C^{13}CD**: 166.5 mg, 52%.

NMR data for **2a-HCCH** matched those in the literature:[90] ^{1}H NMR (200 MHz, C_6D_6, 30 °C): δ 3.30 (d, $^3J_{H-Rh}$ = 2.6 Hz, 2H, *H*C≡C*H*), 2.33 (m, PC*H*, 6H), 1.25 (dvt, $^3J_{H-H}$ = 6.4 Hz, *N* = 13.2 Hz, PCHCH_3). ^{31}P NMR (81.0 MHz, C_6D_6, 30 °C): δ 34.3 (d, $^1J_{P-Rh}$ = 116.6 Hz). Isomerization takes place in C_6D_6 solution at 30 °C. NMR data for **5a-CCH$_2$** matched those in the literature:[34] ^{1}H NMR (500 MHz, C_6D_6, 30 °C): δ 2.85 (m, PC*H*, 6H), 1.32 (dvt, $^3J_{H-H}$ = 6.0 Hz, *N* = 13.5 Hz, PCHCH_3), −0.13 (dt, $^3J_{H-Rh}$ = 1.0 Hz, $^4J_{H-P}$ = 3.5 Hz). ^{31}P NMR (80.95 MHz, C_6D_6, 30 °C): δ 42.3 (d, $^1J_{P-Rh}$ = 135.3 Hz).

NMR data for **2a-D^{13}C^{13}CD**: ^{1}H NMR (200 MHz, C_6D_6, 30 °C): δ 2.21−2.44 (m, PC*H*, 6H), 1.25 (dvt, $^3J_{H-H}$ = 6.2 Hz, *N* = 13.0 Hz, PCHCH_3). ^{31}P NMR (81.0 MHz, C_6D_6, 30 °C): δ 34.4 (d, $^1J_{P-Rh}$ = 116.5 Hz). ^{13}C NMR (50.3 MHz, C_6D_6, 30 °C): δ 67.2−69.4 (m, D^{13}*C*≡^{13}*C*D), 22.2 (vt, *N* = 17.6, P*C*H), 20.2 (s, PCH*C*H$_3$). Isomerization takes place in C_6D_6 solution at 30 °C. NMR data for **5a-^{13}C^{13}CD$_2$**: ^{1}H NMR (500 MHz, C_6D_6, 30 °C): δ 2.70−2.95 (m, PC*H*, 6H), 1.32 (dvt, $^3J_{H-H}$ = 6.0 Hz, *N* = 13.0 Hz, PCHCH_3). Although there should be no high-field signal, centered on −0.13 ppm was a wide doublet of featureless multiplets, $^1J_{H-C}$ = 160 Hz, for **5a-^{13}C^{13}C*H*D**. The total integration of the two peaks corresponded to 0.28 H, meaning that the vinylidene terminal carbon bears 14% H. In the crossover experiment described below the amount of this material was cut to around half, reflecting the fact that in the crossover experiment only half of the starting material was **2a-D^{13}C^{13}CD**. ^{31}P NMR (80.95 MHz, C_6D_6, 30 °C): δ 42.4 (ddd, $^1J_{P-Rh}$ = 135.3 Hz, $^2J_{P-C}$ = 16.2 Hz, $^3J_{P-C}$ = 5.7 Hz). ^{13}C NMR (50.3 MHz, C_6D_6, 30 °C): δ 291.3 (tt, $^1J_{C-Rh}$ = $^1J_{C-C}$ = 57.0 Hz, $^2J_{C-P}$ = 16.0 Hz, Rh=*C*), 87.5−90.5 (m, Rh=C=*C*D$_2$), 23.8 (vt, *N* = 19.9 Hz, P*C*H), 20.6 (s, PCH*C*H$_3$).

Crossover Reaction of [RhCl((*i*-Pr)$_3$P)$_2$(η^2-HC≡CH)] (2a-HCCH) and [RhCl((*i*-Pr)$_3$P)$_2$(η^2-D^{13}C≡^{13}CD)] (2a-D^{13}C^{13}CD). A J-Young NMR tube was charged with **2a-HCCH** (11.8 mg, 0.0243 mmol) and **2a-D^{13}C^{13}CD** (12.2 mg, 0.0250 mmol), and the two solids were dissolved in C_6D_6. The reaction was monitored by ^{1}H NMR spectroscopy. After 18 h, about 60% of the alkyne π-complexes had been converted to vinylidenes, a process completed after 3 days. The amount of **5a-^{13}C^{13}CHD** formed appeared to be about half that obtained from pure **2a-D^{13}C^{13}CD**, as measured by integration of the small, wide doublet of featureless multiplets

(90) Werner, H.; Wolf, J.; Schubert, U.; Ackermann, K. *J. Organomet. Chem.* **1986**, *317*, 327−356.

for **5a-^{13}C^{13}C*H*D**. Thus, the amount of H at the terminal carbon of **5a-^{13}C^{13}CD$_2$** was no greater than when pure **2a-D^{13}C^{13}CD** was used, and therefore H incorporation in Scheme 3 is shown as "ca. 0% H".

Deuterium NMR was performed on a solution made by evaporation of the reaction mixture and redissolution of the residue in C_6H_6 (1 mL) and C_6D_6 (ca. 0.05 mL). A large doublet ($^1J_{D-C}$ = 24.7 Hz) for the $=^{13}C=^{13}CD_2$ moiety of **5a-^{13}C^{13}CD$_2$** was seen, presumably slightly broadened by $^4J_{D-P}$ and $^2J_{D-C}$. In the center of this doublet was a very small peak, which *could* be from **5a-CCH*D***. Deconvolution of the spectrum assuming Lorentzian line shape led to the fit shown in the Supporting Information. The ratio of integral areas for the large peaks of the doublet for **5a-^{13}C^{13}C*D*$_2$** and what may be the singlet for **5a-CCH*D*** was 270 to 1, which would correspond to a molar ratio of 135 to 1. Thus, a 1% detection limit is given for D in **5a-CCH$_2$**.

Ruling Out Isotope Effect as Responsible for Lack of Crossover. In separate silanized and dried J. Young NMR tubes, solutions of **2a-D^{13}C^{13}CD** and **2a-HCCH** in C_6D_6 were allowed to rearrange to the respective vinylidenes at 30 °C in the NMR probe. Comparing rates of disappearance of starting materials showed that $k_{HCCH}/k_{D^{13}C^{13}CD}$ = 1.67, a relatively small effect compared with the low or undetectable D incorporation in crossover experiments above.

Computational Methods. Two methodologies are employed for the principal computational results reported in this study:

1. B3LYP/LANL2DZ calculations were used to carry out (a) the initial conformational analysis on structures **4g**, **4h**, and **4i**; (b) mapping of the reaction surface for structures **2f**−**5f** (Figure 6); and (c) frequency calculations for zero-point energy and thermal contributions to the free energies of **2a**−**5a**, **2c**−**5c**, **2d**−**5d**, and **2e**−**5e**.

2. All tabulated numerical results from the computational work (Tables 3, 4, and 5) are obtained by BLYP/DQZ/UFF ONIOM calculations (labeled BDMM), carried out on structures **2a**−**5a**, **2c**−**5c**, **2d**−**5d**, and **2e**−**5e**, with free energy corrections from the B3LYP/LANL2DZ results above.

The experimental work on imidazolylphosphine complexes used ligand **1b**, which featured a *tert*-butyl group adjacent to the basic nitrogen (Im′). All calculations described in this paper were made tractable by using complexes of imidazolylphosphines **1e** and **1g**, ligands lacking the *tert*-butyl group, where the 1-methylimidazol-2-yl unit is abbreviated as Im; the evidence indicates that this is a reasonable simplification for the systems considered here.[91] The initial calculations were carried out on simplified systems, the [RhCl(H_2PR^1)$_2$](C_2H_2)-derived complexes, with R^1 = H, Im, Ph, *o*-Tol (bearing phosphine ligands **1f**−**1i**, Scheme 2) and with the C_2H_2 group arranged to correspond to each of four minimum-energy species **A**−**D** in Scheme 1, specifically analogues **f**−**i** of **2**−**5** in Scheme 2. The final series of calculations replaced the H atoms in the H_2PR^1 ligands with the *i*-Pr groups present in the experimentally studied compounds and were carried out for each of the species **2**−**5** derived from acetylene complexes [RhCl((i-Pr)$_2$$PR^1$)$_2$]($C_2H_2$) (**2a-**, **2c-**, **2d-**, and **2e-HCCH**, with R^1 = *i*-Pr, Im, Ph, *o*-Tol).

Previous experimental studies on similar systems in this laboratory have been successfully modeled[92] using the B3LYP hybrid density functional and the LANL2DZ basis set, based on Hay and Wadt's effective core potentials.[93,94] This computational approach remains tractable for the present systems, provided that the *i*-Pr groups are replaced by hydrogens in the model compounds. The kinetics and ligand-dependence of the chemistry were therefore initially investigated by B3LYP/LANL2DZ calculations on the [RhCl(H_2PR^1)$_2$](C_2H_2)-derived species.

The final calculations presented in this paper take advantage of the recent benchmark study by Truhlar and co-workers of DFT techniques applied to organometallics.[95] They found that the nonhybrid BLYP method was superior to B3LYP for a broad range of predicted properties. That study relied on the relativistic, compact effective potentials (RCEP) of Stevens et al.[96] and either the accompanying double-ζ basis set or a modified Hay−Wadt triple-ζ basis set, supplemented by Pople's 6-31+G(d,p) basis for the main group atoms. Their findings found little improvement upon extension from the double-ζ (DQZ) to triple-ζ basis. The final optimizations reported here were therefore carried out at the BLYP level with the DQZ basis set. Selected calculations were also carried out at the MP2 and CISD levels (see Supporting Information) to test the sensitivity of our initial results to computational technique.

To simplify computations on the *i*-Pr-substituted species, the experimentally studied molecules were modeled by ONIOM calculations[97] in which the *i*-Pr groups were treated exclusively by UFF molecular mechanics and coupled to the simplified [RhCl(H_2PR^1)$_2$](C_2H_2) system, which in turn was optimized at the BLYP/DQZ level. These ONIOM calculations, designated BDMM in this work, are designed after the IMOMM calculations described by Wakatsuki et al.[41] A series of optimizations were also carried out with a modified version of their IMOMM MP2/MM3 calculations, using a slightly larger basis set (replacing 4-31G by 6-31G* and using the n+1 basis of Hay and Wadt[93,94] and UFF instead of MM3 molecular mechanics); these calculations support the previously reported[41] reaction barrier of 30 kcal/mol. However, Grimme's recently proposed spin-component scaling of the MP2 energy contributions[98] reduces this barrier to 17 kcal mol^{-1}, in rough agreement with DFT calculations that use the same basis set. All calculations were carried out using the Gaussian 03 suite of programs[99] running on a Pentium Xeon cluster under Linux.

Conformational Analysis. Even in the absence of the *i*-Pr groups, there is considerable conformational flexibility in these calculations, particularly for the Im- and *o*-Tol-substituted species. Therefore, 10 distinct initial geometries of the [HRhCl(PH_2Im)$_2$]-CCH hydrido(alkynyl) species **4g** were chosen to survey potential effects of different intermolecular interactions between locations on the imidazole and on the central [HRhCl]CCH framework. The hydrido species was chosen in case its lower symmetry, relative to that of the π-complex and vinylidene isomers, influenced the preferred conformation. Similar but less rigorous conformational tests were carried out for the Ph- and *o*-Tol-substituted compounds (**4h** and **4i**) and for species **2** and **5**, and frequencies were calculated in all cases to ensure that these were minimum energy geometries.

In all cases with R^1 = Im, Ph, or *o*-Tol, the lowest energy conformations of the [RhCl(H_2PR^1)$_2$](HCCH)-derived species **2**−**5** placed both ligand rings roughly anti with respect to each other, each with one CH bond oriented toward the Cl atom for slight electrostatic stabilization. In the case of the Im and Tol ligands, the Cl-oriented hydrogen atom is located on the methyl group. Geometries were subsequently optimized from initial conformations that exploited this stabilizing characteristic. Although the relative energies of these conformers (e.g., E(*gauche*) − E(*anti*) for **2g**)

(91) In other applications of heterocyclic phosphines the steric hindrance at the basic nitrogen is quite important,[32] but as seen in calculated structures here, there is no evidence of the involvement of basic nitrogen in alkyne-to-vinylidene transformation on Rh(I). Therefore, we feel that lack of a ring *tert*-butyl substituent in calculated species should be of little consequence.

(92) Lev, D. A.; Grotjahn, D. B.; Amouri, H. *Organometallics* **2005**, *24*, 4232−4240.

(93) Hay, P. J.; Wadt, W. R. *J. Chem. Phys.* **1985**, *82*, 270−283.

(94) Hay, P. J.; Wadt, W. R. *J. Chem. Phys.* **1985**, *82*, 299−310.

(95) Schultz, N. E.; Zhao, Y.; Truhlar, D. G. *J. Phys. Chem. A* **2005**, *109*, 11127−11143.

(96) Stevens, W. J.; Krauss, M.; Basch, H.; Jasien, P. G. *Can. J. Chem.* **1992**, *70*, 612−630.

(97) Maseras, F.; Morokuma, K. *J. Comput. Chem.* **1995**, *16*, 1170−1179.

(98) Grimme, S. *J. Chem. Phys.* **2003**, *118*, 9095−9102.

(99) Frisch, M. J.; *et al. Gaussian 03*; Gaussian, Inc.: Pittsburgh, PA, 2003. For complete reference, see Supporting Information.

change by as much as 3 kcal mol^{-1}, and more when the *i*-Pr groups are added, the energy difference between any specific pair of conformers along the reaction path (e.g., ΔE_{2-4}(*gauche*) − ΔE_{2-4}(*anti*) for **2g**) was not found to exceed 1.5 kcal mol^{-1}. The ONIOM optimizations of structures featuring (*i*-Pr)$_2$PR^1 ligands yielded no geometries that differed markedly in the central framework from those featuring the PH$_2$R^1 ligands. (A series of BDMM calculations were carried out on structures **2g**−**5g** explicitly to test the possibility of the imidazolyl ligand acting as an internal base to stabilize the HCCH system, but none of these conformers were more stable than the conformers described above.) Minimum energy geometries were then identified by analytical optimizations from initial geometries consistent with the most stable conformers identified in the survey.

Transition-State Optimizations. For the R = H model systems, analytical optimizations of the transition states **TS23** and **TS45** were carried out from initial geometries suggested by the relaxed PES. Frequency analysis confirmed that these were saddle points. This analysis was repeated for **TS34** only in the simplest model system, [RhCl(PH$_3$)$_2$](C$_2$H$_2$), because the minimum associated with **3** is apparently too shallow to contribute substantially to the observed kinetics. (It is for this reason that the transition state that technically connects geometries **3** and **5** is referred to as **TS45** rather than **TS35**.) The transition states in the ONIOM calculations were numerically optimized. The local coordinate most associated with the reaction coordinate near each transition state was identified from the Hessian matrix of the corresponding, analytically optimized [RhCl(H$_2$PR^1)$_2$](C$_2$H$_2$) transition state. These coordinates, the Rh−C2 bond length for **TS23** and the C2−C1−H bond angle for **TS45**, were initially fixed to the value optimized at the level B3LYP/LANL2DZ for the simplified [RhCl(PH$_2$R)$_2$](C$_2$H$_2$) model system. The transition states were then identified in the ONIOM calculations by stepping this parameter in both directions and repeating the partial optimization to determine the location of the peak of the relaxed PES along this coordinate. It was found that the reaction coordinate near **TS23** was too heavily coupled to the Rh−C2−C1 bond angle for this method, and therefore the Rh−C2−C1 angle was also coarsely scanned in roughly 9° increments to improve the predicted **TS23** energy to an estimated precision of 1 kcal/mol.

Wakatsuki et al.'s previous analysis had indicated that the reaction barriers for the unimolecular reaction were too high to account for the observed reaction rates.[41] The present work found a significant decrease in those predicted barrier heights at **TS23** and **TS45** when using DFT methods rather than MP2 calculations, and the lowest predicted barrier height in the preliminary B3LYP/LANL2DZ calculations is 26 kcal mol^{-1}. Results by Hirao[100] and our own vibrational and geometrical benchmarks using RhC and RuO_4 (see Supporting Information) suggest that the DFT methods should be more accurate than the MP2. However, it is only upon adoption of the DQZ basis that the reaction barriers predicted under these conditions become consistent with the experimental results, with similar relative energies obtained using either the B3LYP or BLYP methods. The two major differences between this basis and the LANL2DZ are the implementation of all-electron functions for P and Cl and use of the RCEPs of Stevens et al. rather than the more demanding ECP of Hay and Wadt. The RCEPs were devised using an energy-based optimization scheme, distinct from the orbital-optimization scheme used to develop the Hay−Wadt ECPs, and comprise a relatively compact and efficient expansion of Gaussians to model the pseudopotential.[96] Suresh et al. also predict energy barriers substantially lower than those of Wakatsuki et al.[41] by means of B3LYP calculations, using the Hay−Wadt pseudopotential and basis functions for Rh, and 6-31++G(d,p) basis functions for the main group atoms.[43] The simpler PH$_3$ ligands in their study permit use of a larger basis set than is tractable for the experimentally relevant ligands investigated in the present work.

Acknowledgment. D.B.G. and X.Z. thank the U.S. National Science Foundation for partial support under Grant No. 0415783, Dr. LeRoy Lafferty for help with advanced NMR experiments at SDSU, and Dr. Ashok Krishnaswami of JEOL USA for deuterium NMR experiments. A.L.C. thanks the NSF for partial support under Grant No. CHE-0216563 and Prof. William Richardson for helpful discussions.

Supporting Information Available: Molecular structure of **6c**, CIF files for all structures, details of analysis of spectra of H^{13}C^{13}CH isotopomers, tables of BDMM absolute energies and optimized geometries for **2a**−**5d** and transition states, tables for computational methods comparison and benchmarks, and complete ref 99. This material is available free of charge via the Internet at http://pubs.acs.org.

OM700355R

(100) Yanagisawa, S.; Tsuneda, T.; Hirao, K. *J. Chem. Phys.* **2000**, *112*, 545−553.